HHS Public Access

Author manuscript

Adv Drug Deliv Rev. Author manuscript; available in PMC 2018 April 01.

Published in final edited form as:

Adv Drug Deliv Rev. 2017 April ; 113: 201–222. doi:10.1016/j.addr.2016.09.001.

Opportunities for new CT contrast agents to maximize the diagnostic potential of emerging spectral CT technologies

Benjamin M. Yeh, MD[1], **Paul F. FitzGerald, AAS**[2], **Peter M. Edic, PhD**[2], **Jack W. Lambert, PhD**[1], **Robert E. Colborn, PhD**[2], **Michael E. Marino, PhD**[2], **Paul M. Evans, PhD**[3], **Jeannette C. Roberts, MS**[2], **Zhen J. Wang, MD**[1], **Margaret J. Wong, MD, M.eng.**[1], and **Peter J. Bonitatibus Jr., PhD**[2]

[1]Department of Radiology and Biomedical Imaging, University of California San Francisco, 505 Parnassus Ave, San Francisco, CA 94143-0628

[2]General Electric Global Research, One Research Circle, Niskayuna, New York 12309

[3]GE Healthcare Life Sciences, The Grove Centre, White Lion Road, Amersham, Buckinghamshire, United Kingdom HP7 9LL

Abstract

The introduction of spectral CT imaging in the form of fast clinical dual-energy CT enabled contrast material to be differentiated from other radiodense materials, improved lesion detection in contrast-enhanced scans, and changed the way that existing iodine and barium contrast materials are used in clinical practice. More profoundly, spectral CT can differentiate between individual contrast materials that have different reporter elements such that high-resolution CT imaging of multiple contrast agents can be obtained in a single pass of the CT scanner. These spectral CT capabilities would be even more impactful with the development of contrast materials designed to complement the existing clinical iodine- and barium-based agents. New biocompatible high-atomic number contrast materials with different biodistribution and X-ray attenuation properties than existing agents will expand the diagnostic power of spectral CT imaging without penalties in radiation dose or scan time.

Graphical Abstract

Conventional CT (A, in rabbit) with intravascular and enteric contrast material provides high-resolution depiction of anatomy, but the two contrast materials are indistinguishable except by anatomic context. Modern dual-energy CT (DECT) can improve the conspicuity of contrast agents, but since only iodinated and barium-based agents are clinically available, the enteric and intravascular agents cannot be distinguished from each other, even with DECT. If contrast materials with non-iodine/non-barium reporter atoms are developed, then material decomposition of DECT scans simultaneously enhanced with currently available and the new materials (B, in

Contact information for Benjamin Yeh: UCSF Department of Radiology and Biomedical Imaging, 505 Parnassus Ave M372 Box 0628, San Francisco, CA 94143-0628, ben.yeh@ucsf.edu 415-514-9318 (p).

rabbit) could allow each contrast agent to be differentiated without added radiation dose. In this example case, bismuth enteric contrast material is color coded in green, vascular iodinated contrast is red, and soft tissues are blue.

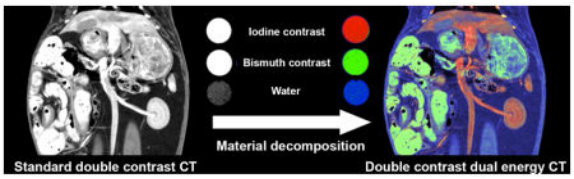

Keywords

dual energy CT; CT contrast material; X-ray contrast material; heavy metal contrast material; spectral CT

1. Introduction

Computed tomography (CT) provides high-resolution anatomic diagnoses for a broad range of disease such that over 85 million CT scans are performed annually in the USA[1] alone, and approximately half of these are performed using intravenous (IV) injected contrast agents. The development of safe radiopaque contrast materials for CT imaging revolutionized the value of this imaging modality for highlighting internal organ lesions and vascular anatomy. Contrast-enhanced CT imaging was quickly adopted as the first-line test for a wide range of critical clinical decisions. As examples, contrast-enhanced CT is essential for patient triage in the emergency setting [2], and also for accurate high-resolution anatomic staging and treatment monitoring of cancer [3], systemic diseases, and vascular disease [4, 5], among others.

Despite the undisputed benefit of contrast material for most clinical CT scanning indications, no substantively new CT contrast material has been approved for clinical use in two decades. Although novel radiodense contrast agents have been proposed in the past decades, the golden age of CT contrast material development appears to have passed. The pace of approvals for CT contrast materials now lags far behind that of radiolabelled agents for positron emission tomography (PET) and single-photon emission computed tomography (SPECT), magnetic agents for magnetic resonance imaging (MR, MRI), and ultrasound (US) contrast agents. The clinical CT contrast agents we use today are all based on tri-iodinated benzene rings (Fig. 1) or colloidal or micronized barium sulfate, and were largely developed in the prior century for general X-ray imaging for fluoroscopic and angiographic use. These agents gained substantially more value when they were adopted for use in CT, which has roughly 40 times the sensitivity of fluoroscopic imaging for radiodense contrast material and provides cross-sectional display of anatomy. Rapid improvements in CT scanner speed, spatial resolution, and radiation dose reduction further expanded the ability of contrast agents to depict lesions in individual organs and the associated blood vessels.

The value of iodinated and barium-based agents was subsequently improved in several ways. Better understanding of contrast material pharmacokinetics[6–10] allowed physicians to

adjust contrast injection rates and CT imaging scan delays to improve the conspicuity of various pathologies. Refinements in the hydrophilic substituents and structure of iodinated agents[11] improved their clinical safety and patient tolerance [12]. However, the fundamental chemical structures of the contrast agents – the tri-iodinated benzene ring and the barium sulfate particle – remained unchanged.

Recently, a fundamental shift in CT technology occurred with the introduction of dual-energy CT (DECT) into every day clinical CT scanners. This groundbreaking technology is FDA approved and every major CT scanner manufacturer now sells clinical scanners with the ability to image objects with two X-ray energy spectra. DECT and photon-counting, energy-discriminating (PCED) CT are two major types of "spectral" CT, in which the unique, energy-dependent attenuating characteristics of materials can provide new diagnostic information[13]. The most-published benefits of spectral CT are reduced image artifacts [14–16], differentiation between tissue compositions [17], and improved detection and quantification of iodine- and barium-based contrast material concentrations [3] with a single pass of the CT scanner. The medical community is gradually embracing DECT for these benefits.

A key to unlocking the capabilities of clinical spectral CT lies in the introduction of new contrast agents designed specifically for these emerging diagnostic imaging technologies. DECT, and future generations of spectral CT scanners, provide the ability to not only detect a given reporter element such as iodine [4], but also to *distinguish between* different reporter elements when multiple contrast agents with different reporter elements are delivered simultaneously or near-simultaneously into the body [18–22]. Our review will cover the basics of DECT and PCED CT technology and the rapidly changing understanding of contrast material usage with DECT, summarize published research on non-iodinated and non-barium agents that could become profoundly useful in the new age of spectral CT, and explore patient-safety challenges that new CT contrast agent development will face.

2. CT technology

2.1. Basics of CT and spectral CT

All CT systems in clinical use today include one or two X-ray source(s) and X-ray detector(s) positioned on a rotating gantry. The X-ray source is activated during rotation of the gantry, and X-ray transmission measurements are collected by the detector at multiple view angles around the scanned anatomical section. The measured data are used to reconstruct cross-sectional images of the scanned anatomy. State-of-the-art CT systems perform a complete rotation of the gantry in 0.25 – 2.0 s, provide 4 – 16 cm of axial coverage (Z-coverage; longitudinal coverage on the patient) per gantry rotation, and acquire ~1000 angular views (projections) of the anatomy during each rotation.

X rays are produced by a large vacuum tube with a rotating tungsten anode. The X-ray energy spectrum that is produced includes a continuum of X-ray energies with a maximum energy (keV) that corresponds to the peak operating voltage (kVp) of the X-ray tube (typically from 80 kVp to 140 kVp), and a minimum energy of approximately 30–40 keV (Fig. 2). The lower energies are typically filtered out before reaching the patient, because

they would not penetrate the patient and thus would contribute to patient radiation dose without contributing to image quality[23]. We emphasize the distinction between the terms “kVp” and “keV”, as both units are common in CT imaging terminology. The integral of the individual photons is termed the X-ray photon fluence; similarly, the integral of the energies of all photons in the spectrum is the energy fluence. The photon fluence determines the quantum noise in the CT image (the second important noise source in CT images is electronic noise from the X-ray detector). The energy fluence, in combination with the energy-dependent attenuation of the materials in the patient, determines the CT image contrast as well as the radiation dose to the patient. Typical clinical CT X-ray spectra were estimated using XPECT software[24] and are shown in Fig. 3A, and are plotted in terms of energy fluence. These curves were produced by simulation using typical CT system parameters and a typical patient diameter; however, the same X-ray tube current (mA) was used to simulate the spectra at each kVp. Clearly, the higher kVp spectra produce dramatically more energy (per mA) than the lower-kVp spectra; therefore, it is critical for the radiologist to carefully adjust both kVp and mA in order to use the lowest radiation dose that is required to obtain the necessary diagnostic information, in light of the patient size and clinical task. When evaluating CT system performance at different kVp and using different contrast materials, it is often convenient to normalize the spectra to equal integrated energy; Fig. 4A are the same data as Fig. 3A, but normalized.

During imaging, X-rays are attenuated by the tissue along the paths from the X-ray source to each picture element (pixel) in the X-ray detector. The attenuation depends on the mass attenuation coefficient[25] (MAC; μ/ρ cm^2/g) and the density (ρ g/cm^3) of all materials on that path, and the path lengths through each material. The MAC of each material is the linear attenuation coefficient (LAC; μ; cm^{-1}) per unit density. The MAC is unique for each material and is a function of energy. The MAC decreases monotonically with increasing energy unless the material contains an element with a K-edge within the X-ray spectrum. (The K-edge refers to the minimum energy required to liberate a K-shell electron from the atom.) Typically, no such K-edges are present within biological tissues for the diagnostic imaging X-ray spectra (40 to 140 keV). The K-edge energies for iodine (I), barium (Ba), and gadolinium (Gd) are 33 keV, 37 keV, and 50 keV respectively[26] and are near the low end of X-ray spectra used for clinical CT. However, some proposed contrast agent elements have K-edge energies well within clinically-used X-ray spectra; we will discuss these later. Fig. 3B shows the MACs for three elements that are reasonable to consider for use in CT contrast agents from a cost and availability perspective; these are chosen for illustrative purposes because their K-edges span the range of the clinical spectra.

As X-rays pass through the patient, they are attenuated according to the Beer-Lambert Law:

$$I_T = I_0 e^{-\mu l}$$

which can be re-written as

$$I_A = I_0 (1 - e^{-\mu l})$$

where I_T is the intensity of the X-rays transmitted through the patient, I_A is the attenuated intensity (not transmitted through the patient), I_0 is the incident intensity, μ is the LAC of the material, and I is the path length through that material. Note that I_A, I_0, and μ are energy dependent. The Beer-Lambert Law applies to each discrete energy, and the total attenuation obtained with a polychromatic energy source as is used with clinical CT is the integral over energy. For simplicity, we have omitted the notation (E) from these quantities in the above and subsequent equations. To best understand how a particular X-ray spectrum interacts with a certain material, it is important to appreciate that the material's attenuation is an exponential function of its attenuation coefficient. We can more directly evaluate the attenuation of a material if we calculate an attenuation factor

$$F = 1 - e^{-\mu l} = 1 - e^{-\frac{\mu}{\rho}\rho l}$$

where F is the attenuation factor, μ/ρ is the MAC, ρ is the material's density, and I is the path length through the material. For purposes of illustration, in Fig. 4B, we have plotted this attenuation factor for the materials shown in Fig. 3B, using ρ = 0.01 g/cm (approximating a contrast agent's clinically-relevant active element concentration of 10 mg/mL) and I = 2 cm (approximating a large vessel).

With the curves of Fig. 4A and Fig. 4B, we can appreciate the attenuation of specific spectra by selected materials, by direct multiplication. Fig. 4C and Fig. 4D are examples using the 80 kVp and 140 kVp spectra, respectively. Fig. 4E shows the CT image contrast that results from the effects illustrated in Figures 4C and 4D. Because iodine's k-edge energy is well below the mean energy of both spectra shown in Figs 4C and 4D, the image contrast produced by iodine when using a 140-kVp tube potential is substantially reduced (by approximately half) compared with that obtained when using 80 kVp. Due to the effects of bismuth's L-edge when using 80-kVp tube potential and its kedge when using 140 kVp, bismuth has somewhat similar image contrast at these tube potentials, but does exhibit approximately 13% lower image contrast when using 140 kVp versus 80 kVp. Tantalum produces nearly equal image contrast at these two tube potentials because its k-edge energy occurs at 67 keV, which is near the center of the clinically-relevant X-ray energy range.

To date, all commercial CT systems use energy-integrating X-ray detector technology: the detected signal is the integral of the energy converted from detected photons at all X-ray energies. Within the detector, a scintillator converts X-ray energy to visible light energy, which illuminates a photo-diode to generate an electric charge, which is digitized. Using the measured projection data, the LAC of the material within each volumetric picture element (voxel) in the imaged anatomy is reconstructed. The numerical values assigned to each voxel in CT images are referred to as CT numbers, in Hounsfield Units (HU), and are defined as the LAC of the material in the voxel, normalized to the LACs of water and air (as calibrated on that system), such that air is assigned a CT number of −1000 HU and water assigned 0 HU[27]:

$$HU = 1000 \times \frac{\mu_{material} - \mu_{water}}{\mu_{water} - \mu_{air}}$$

The underlying principle of DECT involves exploiting the unique relative differences in X-ray attenuation of individual materials when imaged at low versus high X-ray tube voltages, as a means to distinguish between materials in CT images. This is different from conventional single-energy CT (SECT), which provides images based on the X-ray attenuation at one X-ray tube voltage, and as such is unable to distinguish between different materials that are present – only the effective LAC can be estimated; this cannot be separated into the LACs of specific constituents that may be present in a given voxel.

This concept of dual-energy CT for material characterization was realized early in the development of CT. In fact, Godfrey Hounsfield described the use of dual-energy CT to distinguish iodine from calcium in the original paper describing CT[28]. Soon after this initial description of CT several potential applications were outlined[29–33], and clinical application of DECT was initially reported in 1978[34]. Since early CT scanners required substantial time between acquisition of imaging data using different tube potentials, DECT imaging of contrast material which may change rapidly in distribution after injection was not feasible. As such, initial clinical dual-energy applications focused on unenhanced scans, such as to quantify bone mineral density[35], liver iron content[36, 37] or to characterize the mineral composition of unenhanced tissues[38]. However, unlike single-energy CT applications, none of the early DECT applications gained widespread use, likely due to the limit of added diagnostic value of quantitative tissue composition characterization compared to the rich anatomic data that is provided by simple single-energy CT, particularly with contrast material enhancement; the cumbersome approach to DECT which required substantial manual effort to make computations; and the poor image co-registration of the low- and high-kVp images.

Modern clinical DECT scanning overcomes the early limitations by providing rapid sequential or simultaneous acquisition of CT datasets that represent the attenuation associated with two different X-ray spectra, one with a lower mean photon energy (usually obtained by operating at 80 kVp) and one spectrum with a high mean energy (usually obtained by operating at 140 kVp). The datasets are then compared through automated or semi-automated post-processing algorithms to generate material-specific images. In DECT, an additional X-ray filter is sometimes used to tailor the high-kVp spectrum in order to provide improved separation between the two spectra.

To understand the physics that enable DECT, we must consider the MAC in more depth. For a more complete resource on x-ray interaction physics, we refer the reader to Beutel, Jacob, Harold L. Kundel, and Richard L. Van Metter. “Handbook of Medical Imaging, volume 1: Physics and Psychophysics.” (2000). Chapter 1 pp 17–57 [39], from which the following paragraphs are summarized. The MAC of a material depends on its physical density, due to Compton scattering, and on its effective atomic number, due to the photoelectric effect. Compton scattering is an inelastic scattering phenomenon whereby a photon interacts with and displaces an outer shell electron, losing energy and being deflected in the process. The

probability of this interaction depends on the electron density of a material, which is dependent on its physical density but independent of its atomic number (Z). Compton scattering is largely independent of X-ray energy over the diagnostic energy range, which is approximately 40–140 keV.

On the other hand, the photoelectric effect is an inner electron (K or L)-shell interaction, whereby an incident X-ray photon is completely absorbed, and a photo-electron is ejected. For this effect to occur for a K-shell electron, the incident photon requires energy greater than or equal to the discrete binding energy of the K-shell electron. This binding energy is characteristic for each element, and results in a step increase in X-ray attenuation at the so-called K-edge energy, at or above which photons can be absorbed by the K-shell. K-edge energies are expressed in keV, and have a large effect on attenuation, particularly for elements with high atomic numbers. This is the case for current elements used in CT contrast agents, whose K-edge energies are just below the typical CT spectrum. In addition to providing high image contrast at SECT, this dependency can be harnessed for use at DECT. For instance, the K-edge energy of iodine is 33 keV, nearer to the mean photon energy of the low-kVp spectrum (~56 keV) than that of the high-kVp spectrum (~76 keV) [40]. This results in a large attenuation in the low-kVp image, and a much lower attenuation in the high-kVp image. The difference is sufficient in the case of iodine to produce a nearly two-fold difference in CT number at DECT[41]. As a second example, the K-edge of tantalum is 67 keV, near the mean photon energy of the high-kVp X-ray spectrum. This increases the attenuation in the high-kVp image, and when combined with the other photon interactions, results in a similar CT numbers at low- and high-kVp images[42]. The relative difference in low- to high-kVp CT number ratios allow for the contribution of two different materials to be determined at DECT material decomposition post-processing[19, 43].

By using the LACs of selected materials in the CT image processing software, both CT numbers and material concentrations can be assigned to the reconstructed data. The greater the difference in LAC profiles between two materials, the higher the fidelity of these material-specific images, and the more accurate the separation at DECT[42]. Contrast materials with a greater difference in LAC profile compared to those of soft tissue or bone are more readily differentiated from tissue or bone, respectively, than contrast materials with an LAC profile closer to those of soft tissue or bone.

A complementary capability of DECT is the reduction of artifacts such as beam-hardening artifacts. Beam hardening is a phenomenon where low-energy photons are attenuated to a greater extent than are higher-energy photons as the X-ray beam traverses the imaged object[44]. This preferential loss of lower-energy photons increases the mean photon energy of the spectrum (“hardening” the beam), particularly for thick portions of anatomy or when highly-attenuating material is imaged. The hardened X-ray spectrum results in lower-than-expected CT numbers, which reduces the accuracy of quantitative measurements. The effect is more pronounced in larger patient sizes since the X-ray spectrum is more highly attenuated when it traverses longer path lengths[45]. Interestingly, since beam hardening occurs for all materials roughly proportionally, beam-hardening artifacts do not substantially affect material decomposition at DECT. Also, since beam hardening is an energy-dependent phenomenon that can be modeled in dual-energy data analysis, beam hardening can ideally

be eliminated in the image formation process[46]. As an extension, metal artifacts caused by beam hardening have also been successfully mitigated using DECT.[47]

2.2. Types of clinical DECT scanners

Five types of clinical DECT scanners have been realized since practical DECT was first introduced clinically in 2006. Each implementation presents a fundamentally different hardware design approach with distinct advantages and limitations (Fig. 5).

The most straightforward design uses a rotate-rotate acquisition and is offered by GE (Revolution CT, GE Healthcare, Milwaukee, WI, USA), Siemens (Somatom Definition Edge, Siemens Healthcare, Forchheim, Germany) and Toshiba (Aquillon One, Toshiba, Tochigi, Japan) [48]. With this technique, an acquisition using a low-kVp spectrum is performed, followed by a second acquisition using a high-kVp spectrum (Fig. 5A). Rotate-rotate systems require no hardware modification and can thus be implemented on standard SECT systems. However, they are limited by the long inter-scan delay required between the two separate scans. Inter-scan delay may result in substantial changes in the distribution of intravenous contrast material and may result in image co-registration issues since visceral organs commonly move, and depth of respiration may change between scans. As such, rotate-rotate DECT acquisitions are generally limited to exams that do not require administration of contrast material and where the location of viscera is relatively fixed, such as kidney stone characterization, musculoskeletal uric acid deposition evaluation, or for the reduction of metal artifacts [40, 49]. Since modern CT scanners provide wide Z-coverage (up to 16 cm) and fast rotation time (down to 0.25 s), the limitations of rotate-rotate DECT acquisitions such as voluntary and involuntary patient motion may be somewhat mitigated, although contrast-enhanced imaging still remains difficult, particularly during the arterial phase where the extent and location of contrast enhancement changes rapidly.

Second, Dual Source CT (DSCT; Siemens Somatom Definition, Flash and Force) employs two separate X-ray source-detector pairs, mounted ~90° apart in the CT gantry, operating simultaneously at different kVp (Fig. 5B). Separation between the low- and high-kVp datasets is excellent as the two X-ray sources can be optimized and filtered independently. However, purchase and operating costs are high due to the two separate source-detector pairs. Furthermore, physical space in the gantry limits the acquisition field of view (FOV) of one of the two X-ray source and detector pairs[50, 51]. This FOV was restricted to 26 cm in the first-generation DSCT scanner (compared to 50 cm or more for a standard CT scanner), but has since increased to 33 cm and now 35 cm in more recent versions. Temporal resolution is sufficient for all types of acquisition, however the ~90° angular difference between the source-detector pairs still implies a 71–95 ms time delay between matched images, which may cause some misregistration artifacts that result from general patient or internal organ motion[49]; the artifacts arise from slightly different positions of the same anatomy during acquisition of low- and high-kVp projections.

Third, rapid-kVp-switching DECT (GE Discovery CT 750HD; Revolution HD) uses a single X-ray tube that switches between low and high kVp at sub-ms intervals to acquire dual-kVp data with a single rotation of the gantry (Fig. 5C). The temporal correlation between low- and high-kVp projections is excellent due to the minimal time interval between low- and

high-kVp acquisitions. It is difficult to increase the spectral separation by use of a tin filter in this type of scanner because it is impractical with present technology to insert and remove such a filter in synchronism with the kVp switching, as the kVp alternates many hundreds of times per second. Furthermore, it is technically difficult to apply high tube current for the low-kVp projections and low tube current for the high-kVp projections, as would be preferred. This can be mitigated by modifying the detector signal integration interval for the low- and high-kVp X-ray projection data acquisitions; however, difficulties may remain for obese patients, where low-energy X-rays are excessively attenuated.

Fourth, multilayer detector CT (IQon; Philips Healthcare, Eindhoven, The Netherlands) utilizes a single-spectrum X-ray source and a “sandwich” type, two-layer detector (Fig. 5D). The front layer of the detector (closest to the patient) is relatively thin and predominantly absorbs the low-energy photons to acquire the low-mean-energy projection data, while the back layer of the detector is highly efficient and absorbs the remaining high-energy photons. With simultaneous acquisition of low and high-mean-energy projections, the temporal correlation between low- and high-mean-energy projections is perfect. This single, non-switching implementation allows for straightforward DECT use in standard clinical practice without the need to “turn on” dual-energy mode because the dual-energy data are acquired for all scans. However, spectral separation may be less robust due to the fixed nature of the design and substantial spectral overlap between the low- and high-mean-energy projections.

Finally, split-beam CT (Siemens Somatom Definition Edge) uses a single X-ray source operating at 120 kVp, and a two-part X-ray filter mounted along the Z- (patient length) axis (Fig. 5E). One part of the filter, composed of gold, preferentially blocks high-energy X-ray photons due to its K-edge of 81 keV, resulting in a reduced mean X-ray energy for half of the beam. The other part of the filter is composed of tin and preferentially blocks low-energy X-ray photons, resulting in a relatively high mean energy for the other half of the beam. By using a low-pitch helical scan trajectory, a given anatomical region sees incident X-rays from both the low- and high-mean-energy parts of the beam during a scan, and both sets of images can be reconstructed. This implementation is the simplest of the three types of simultaneous acquisition systems, but as with multi-layer detector DECT, the two energy spectra are not well separated due to the single-kVp X-ray source that is used. In addition, the temporal correlation between low- and high-mean-energy projections is not ideal because the projections corresponding to the same anatomy are nominally one rotation apart. Finally, the split beam reduces the system’s Z-coverage, which reduces the speed of scanning.

2.3. Material decomposition

The main breakthrough in DECT that would benefit from high-Z contrast material development is material decomposition (MD), which refers to digital processing of the DECT data to represent the scanned anatomy as fractions of two or more “basis” materials. Material decomposition first requires knowledge of the LACs of the chosen basis materials at the relevant X-ray energy range, approximately 40–140 keV. These are common physical properties, available from the National Institute of Standards and Technology (NIST) for all elements and many common compounds. With knowledge of the X-ray spectra at low- and

high-kVps and the LACs of the basis materials, the relative attenuation of these materials in the low- and high-kVp data can be calculated. There are two general methods for performing MD. Material decomposition can be performed on reconstructed images (image-based MD) for all DECT implementations. Material decomposition is performed on projection data (projection-based MD) for DECT implementations in which low- and high-mean-energy projections are temporally and spatially co-registered – e.g. multilayer-detector DECT; photon-counting, energy-discrimination CT (to be discussed later), and, to a practical extent, rapid-kVp-switching DECT. The primary advantage of projection-based MD is that LACs of each material can be more accurately incorporated into the MD model, and therefore image quality can be improved, i.e., ideally, beam-hardening artifacts can theoretically be eliminated entirely. In projection-based MD, the decomposed projection data are used to generate material density images, which can be combined to generate virtual monochromatic (VM) images, as if CT data had been acquired with an X-ray spectrum comprising a single energy. In image-based MD, the low- and high-kVp projection data are used separately to reconstruct images, and MD can be performed from those images. Alternatively, the relative attenuation difference between the low- and high-mean-energy CT numbers for of a material, known as the dual-energy ratio (DER), can be used to identify and quantify the presence of the material in the image data.

Two-material decomposition models the attenuation of the object as being composed of varying proportions of exactly two predefined constituent materials. It is commonly used for its simplicity and sound physical principle; with the information available from two X-ray spectra, the fractions of two materials can be ascertained. However, materials that are not one of the basis materials are assigned (fractionally) to both basis-material images; this can lead to ambiguous results for some materials. Multi-material decomposition is also a common processing technique, but requires the assumptions that image voxels are characterized by combinations of constituent materials and a volume conservation constraint, that is the sum of the volumes of the constituent materials must equal the volume of the overall mixture. For dual-energy analysis, this gives three known conditions for three unknown materials, and is thus solvable as a simultaneous equation.[52] For more than three materials, exact analytical solutions do not exist, and numerical optimization methods are used.[53]

Material decomposition is typically performed automatically by the scanner software through two-material decomposition, resulting in material-image pairs that represent basis material concentration, or material-image triplets through three-material decomposition. A typical basis-material pair includes water and the administered contrast material, usually iodine. With its K-edge energy at the lower end of the DECT X-ray spectra, iodine has a very high DER when analyzing low- and high-mean-energy reconstructions, and can thus be readily separated from most biological tissues, the exception being calcium-containing tissues such as bone and calcium deposits. This is because the LAC of calcium lies between those of iodine and water. Both the “water” and the “iodine” basis-material-concentration images have diagnostic uses. Water-only images (with the iodinated contrast material suppressed) can be used as virtual unenhanced images and in some cases can eliminate the need for a true non-contrast exam phase, saving both patient radiation dose and exam time. [54–56] The iodine-only images (with the background water suppressed) highlight the

distribution of the contrast material and also enable quantification of iodine concentration in mg/mL. This increases diagnostic power compared to standard metrics based on CT numbers alone.[57] Iodine-only images are also able to highlight low concentrations of iodine that may be difficult to detect in SECT images. Other common basis-material pairs include calcium/water, which allows visualization of gout crystals,[58] and iron/water, which allows quantification of iron in the liver or other visceral organs.[59] Three-material decomposition has been implemented with basis-material-triplets such as iodine/calcium/water for coronary plaque evaluation,[60] and iron/iodine/water for the quantification of liver fat.[61]

Other material decomposition basis-material-pairs and -triplets are currently of less clinical benefit. Notably, the currently available CT contrast agents based on iodine and barium cannot be separated from each other at DECT because their LACs are nearly identical. This is because iodine and barium have nearly the same atomic number (53 and 56, respectively). As such, these agents are not complementary at DECT and, much like with conventional SECT, the similar attenuation properties of iodine and barium confound unique identification of these agents in reconstructed images and may cause diagnostic ambiguity. Development of contrast materials with reporter elements that attenuate X-rays strongly and which have substantially different LACs than iodine and barium would allow DECT to provide high-resolution images of each contrast material with a single pass of the CT scanner[42]. Such images promise to provide substantially greater diagnostic value than is possible with current agents, at equal or possibly lower radiation and/or contrast agent dose.

2.4. Potential DECT upgrades

The clinical adoption of DECT continues to grow. Some tradeoffs are seen with different DECT platforms, and include increased beam-hardening image artifacts, limitations in material decomposition, reduced temporal resolution for system types with compromised temporal correlation, and issues with workflow due to large amounts of image data. Nevertheless, future improvements promise to improve the capabilities of DECT on many levels. These improvements can be broadly divided into hardware and software improvements, and the following aspects could improve the overall fidelity of DECT imaging:

1. High-resolution imaging to enable classification of smaller features;
2. Concurrent low- and high-mean-energy acquisitions for perfect temporal and spatial registration of acquired data;
3. Improved spectral separation between low-energy and high-mean-energy measurements to improve the fidelity of the material decomposition process;
4. Transparent collection of energy-dependent imaging information, using standard imaging protocols (same X-ray tube voltage and current) and dose reduction techniques (X-ray tube current modulation), to use clinically as needed; and
5. Enhanced material decomposition and reconstruction algorithms to reduce noise and improve the accuracy of the material density estimates.

2.4.1. Hardware upgrades—Several technical advances in CT hardware will likely improve the performance of DECT imaging over the next few years. Although potential hardware improvements depend in part on the type of DECT implementation for a given system, future hardware improvements include improved separation of the low- and high-kVp X-ray spectra, faster CT gantry rotation speeds, and advances in anti-scatter grid technology.

First, improved selective filtration of the X-ray spectra would enable superior spectral separation of two or more X-ray spectra, and in turn offer improved fidelity of material-specific images. Aggressive filtration of the X-ray spectrum to limit the transmission of low-energy photons in the high-kVp spectrum is achieved by one manufacturer using tin as the filtration material. (Fig. 6) In addition to offering improved spectral separation when using 80- and 140-kVp X-ray spectra,[62] additional tin filtration could also provide good spectral separation with improved image quality when using 100 kVp rather than 80 kVp for the low-kVp source of a dual-source DECT scanner.[63] This option mitigates the possibility of insufficient X-ray penetration of the low-kVp radiation through large patients, and may offer lower image noise with adequate spectral separation in many DECT applications; however, this solution also reduces the separation between the low- and high-kVp spectra[64].

Second, the increased rotation speed of modern CT gantries will improve temporal resolution, temporal correlation of the low- and high-kVp projections for rotate-rotate, dual-source, and split-beam CT implementations, and reduce motion artifacts[65, 66]. The current fastest gantry rotation times are approximately 0.27 seconds per revolution for all CT manufacturers, and a rotation time of 0.2 s is planned by at least one manufacturer. Combined with the increased Z-coverage, currently up to 16 cm, this implies very fast imaging of large anatomical sections. For example, complete cardiac scans are now possible using a single axial rotation during the diastolic phase of one heartbeat[67]. Although these high-speed scan protocols are not always achievable at DECT due to tube current limitations, advances in tube power may soon make these ultrafast scans available for all protocols.

Third, advances in anti-scatter grids directly in front of the detector could improve the signal-to-noise properties of the CT projection data and improve image quality[68]. Anti-scatter grids, also called post-patient collimators, are geometrically aligned with the X-ray source and thus attenuate scattered photons coming from other angles, which are detrimental to the image formation[69]. Traditionally, these grids were simple in design; however, with the advent of wide-collimation scanning of up to 16 cm, the increased proportion of scattered photons has required careful consideration[70]. Focused, two-dimensional (2D) anti-scatter grids have therefore been introduced, which have septa running parallel to both detector rows and columns[71, 72]. These are especially important for DSCT, where the simultaneous output of the two source-detector pairs produces a greater amount of scattered radiation[73]. Continued optimization of these grids will lead to improved signal-to-noise properties in the CT image data.

Finally, improvements in X-ray tube performance in the rapid-kVp-switching architecture could reduce noise in DECT images by increasing the X-ray tube current used for the low-kVp projections.

2.4.2. Software upgrades—Several software technologies are in development that will further enhance the diagnostic capabilities of DECT. First, more sophisticated material decomposition techniques will enable separation of more materials than the current basis-material-pairs or -triplets approach. Care must be taken with this multi-material decomposition due the absence of exact, analytical solutions; however, the ability to determine more than three materials will likely expand and enhance the information provided by DECT.

Further technical advances that are being developed for CT in general will also benefit DECT. These include refinement of automatic exposure control (AEC) and iterative reconstruction (IR) technologies. AEC has enabled CT dose reduction of up to 50% by tailoring the X-ray tube current to an individual patient's anatomical and attenuation properties. Within the last five years, automatic selection of the X-ray tube voltage, in addition to the tube current, has also been introduced. Eventually, this automatic tube voltage selection may extend to DECT protocols, with patient-specific selection of 70–100 kVp for the low-kVp source, and 140–150 kVp for the high-kVp source, with or without additional beam filtration. This will improve both dose optimization and material separation capabilities of DECT, moving it towards the patient-specific protocol definition that currently remains the preserve of SECT.

Recently, clinical implementation of IR can allow CT dose reduction of 50% compared to conventional filtered back projection reconstructions[74]. All CT manufacturers now offer one or more IR packages, some of which are more effective than others. This technology can also be leveraged for dual-energy CT imaging, providing a framework to enable joint estimation of basis material density information. These approaches could reduce imaging noise, while improving the fidelity of material characterization by incorporating appropriate physical models in the image reconstruction process. The ultimate benefit of these approaches will be more accurate basis-material density estimates, taking us one step closer to quantitative CT. A long-term goal has been for reconstructed CT numbers (HU) to be more quantitative, i.e. characteristic of disease detection and assessment, irrespective of the type of CT system used to acquire the data. A common limitation with IR remains its reconstruction time, and with increases in the computational power available, more sophisticated IR methods that model more aspects of CT physics will continue to improve image formation.

Improvements in image display and speed of image reconstruction will address current concerns of reduced clinical throughput. Automation in image reconstruction as well as innovations in the graphical user interface for workstations and clinical picture archiving and communications software (PACS) are needed, and will decrease the time required to read and interrogate the rich data from DECT scans.

These ongoing hardware and software advances will continue to ensure that DECT requires equal radiation dose or lower dose than SECT, eliminating one of its main disadvantages when first introduced. Though several technical upgrades have been outlined here, they all represent incremental advances of an already established technology. A profound technical advancement of DECT beyond those discussed above is likely to come in the form of true spectral discrimination, such as with photon-counting, energy-discriminating CT.

2.5. Photon-counting, energy-discriminating CT

The first investigational CT systems based on photon-counting energy-discriminating (PCED) detectors was evaluated almost a decade ago[75, 76]. More recently, whole-body-sized PCED-based systems are now being evaluated[77, 78]. A conceptual representation of this approach is shown in Fig. 7. Although PCED detectors remain experimental, they promise to reduce radiation dose and improve material decomposition at CT by addressing fundamental limitations of the energy-integrating (EI) detector currently used in all clinical CT systems. Since EI detectors sum all of the energy deposited in each of the detector's pixels, high-energy photons are inherently weighted as more important in measurement data since they contain more energy; however, for materials that do not have a K-edge within the X-ray spectrum being used, high-energy X-ray photons carry less contrast information given the linear attenuation coefficient of low-Z materials, which decrease monotonically with energy.

An alternate X-ray detection mechanism that has been in development for over ten years is PCED detector technology. This type of detector uses a monolithic sensor of a direct-conversion material, typically cadmium telluride (CdTe) or cadmium zinc telluride (CZT) crystal. As suggested by its name, a direct-conversion material converts X-ray energy directly into electric charge (without the intermediate conversion to visible light as with EI detectors). Biased electrodes then collect the electric charge on the surfaces of the sensor. In ideal circumstances, a PCED detector detects each photon that is incident upon the detector, determines its energy (proportional to the detected electric charge), and records the event by incrementing a counter representing one of N energy bins. Using the multi-energy information, novel weighting schemes can be used to improve the contrast-to-noise ratio (CNR) of materials in reconstructed images. As mentioned above, EI technology inherently weights high-energy X-ray photons as more important; but these photons carry less contrast information when low-atomic number (Z) contrast agents are used. However, the photon counts in the N energy bins acquired with PCED detectors can be weighted as appropriate to maximize the imaging contrast-to-noise ratio. As such, X-ray photons can be weighted depending on the energies that are important for the contrast agent in use.

PCED detectors offer several other benefits when compared to their EI counterparts. First, a low-energy threshold can be chosen below the diagnostic energy range (i.e. below ~40 keV). Electronic noise in the detector would produce the same signal level as photons in this low-energy range, but because there are no transmitted photons in this energy range, we can exclude this range entirely and essentially eliminate electronic noise. This results in superior low-signal performance - a must for low-dose screening protocols. Unlike EI detectors where each individual detector pixel is separately fabricated and coated with a reflector

material, direct-conversion materials use patterned electrodes on the surface of a monolithic sensor; this characteristic results in improved detection efficiency, enabling use of detectors with at least twice the spatial resolution of existing EI detectors. Another benefit of PCED detectors is the ability to characterize the energy of each detected photon. This information enables reconstruction of not only the LAC of the material in each voxel, but, like DECT, provides the ability to estimate the material composition within each voxel. As discussed above, EI detectors are typically used at DECT to acquire projections at two kVps, enabling characterization of the materials in each voxel as a linear combination of two specified basis materials, such as bone and water, or iodine and water. However, PCED detectors can acquire projection measurements for three or more energy bins; hence, it becomes possible to characterize the composition of each voxel as a combination of three or more basis materials, such as water, bone, and iodine, or water, iodine, and another contrast agent, without the assumption of volume conservation or use of numerical optimization. As such, it becomes possible to devise novel imaging protocols that better discriminate between multiple contrast materials to improve disease diagnosis.

In summary, PCED detectors offer the benefits of (1) higher spatial resolution for visualizing smaller features, (2) better X-ray detection efficiency and low-signal performance to enable population radiation dose reduction, (3) multi-energy information to facilitate novel schemes to reduce required contrast material dose or improve material characterization, and (4) material information that is always available using existing optimized data collection protocols (dose modulation protocols) without *a priori* intent. The key challenges that need to be met for photon-counting CT to expand its breadth of imaging applications include improvements in detector stability and count rate capability, and reduction in cost of the detectors.

2.6. Phase-contrast CT

Current clinical X-ray-based imaging displays the magnitude of the X-ray attenuation caused by a portion of the patient's anatomy. But, X-rays are nothing more than a form of electromagnetic radiation, just as are radio waves and visible light. As is the case with all electromagnetic radiation, X-ray photons exhibit both particle and wave properties, the latter comprising both a magnitude and phase. Phase-contrast CT exploits the wave property of X-rays and, for example, estimates the phase difference between acquisitions with and without an object placed in the X-ray beam.

While the technical basis for estimating X-ray phase differences is beyond the scope of our review, phase-contrast CT is of interest because of its ability to distinguish between materials [79, 80]. Unlike standard X-ray attenuation imaging that depends on both the electron density and effective atomic number of materials in the X-ray path, X-ray phase information enables direct estimation of the electron density only of the materials in the X-ray path – providing a distinct contrast mechanism. As such, one can envision scenarios where materials are indistinguishable in standard attenuation imaging due to combined effects of electron density and effective atomic number, but are easily separated with phase contrast information. (The reverse scenario is also possible.) Although research is underway, phase-contrast CT technology currently is limited to very small imaging fields of view, does

not operate at clinical CT energies (up to 140 keV), and requires additional acquisitions to obtain the requisite data, which may increase dose and/or extend the data collection time [79, 81].

3. DECT visualizes contrast material differently than does SECT

Two only two active elements used in current CT contrast agents are iodine (Z=53) and barium (Z=56); these elements have very similar MAC curves, with good X-ray attenuation at lower energies (see iodine's MAC in Fig. 3B). This means that iodine and barium are much more effective when imaged at lower kVp (e.g. 80 or 100 kVp) rather than 120 or 140 kVp. In light of this, the recent trend in SECT has been to use lower kVp when possible. However, lower-energy X-ray photons are less able to penetrate through thick body parts, and therefore, when imaging average-sized and larger adult patients, lower-kVp scanning is not feasible.

The primary benefit of low-kVp CT and DECT is the improved detection of iodine and barium contrast material. The CT number of any given concentration of iodinated or barium contrast agent is approximately 70 to 90% higher when imaged at 80 kVp than when imaged at 140 kVp, and this difference can be even greater on DECT iodine density maps or low-keV image reconstructions. The increased conspicuity of iodinated contrast material when using DECT or low-kVp SECT allows physicians to select among the following potential benefits:

1. Reduced contrast material dose without sacrificing contrast material conspicuity;
2. Superior lesion detectability (improved CNR) with standard contrast material dose;
3. Reduced radiation dose without loss of CNR in the CT image; or
4. A combination of these benefits.

Each of these approaches is a topic of active clinical investigation. In addition, DECT is commonly utilized to provide virtual unenhanced CT images, with the contrast material digitally suppressed.

3.1. DECT using reduced iodine dose

The most common clinical consideration that limits the use of intravenous iodinated contrast material for CT imaging is the fear of contrast-induced nephropathy (CIN) or contrast-induced acute kidney injury (CIAKI), which is a worsening of renal function that occurs within 48 hours of intravascular contrast material injection. The prevalence and severity of CIN remains under intense investigation[82], but is traditionally believed to occur at a rate of between 7 to 11%, with a higher incidence seen in patients with poor renal function[83]. While most cases of CIN are transient and do not result in chronic renal failure, a fraction of patients may develop complete renal failure that requires dialysis treatment with associated poor clinical outcomes. Smaller doses of intravascular iodinated contrast material are associated with a lower risk of CIN.

Since DECT and low-kVp SECT enable improved detection of iodine contrast material compared with conventional SECT, smaller doses of iodinated agents may be used in routine or high-risk patients. Dual-energy CT utilizing smaller doses of iodinated contrast material is desirable for angiographic studies where the primary goal is to assess arterial patency and anatomy. In part, this success is related to the relatively small size of the intra-arterial volume. For example, a successful application of DECT using lower contrast dose is DECT pulmonary angiography to evaluate for potentially deadly pulmonary embolic disease[84]. For such scans, DECT provides high image contrast from iodinated contrast material within blood vessels to define the size, shape and distribution of 2- to 12- mm diameter intravascular embolic thrombi. In addition, DECT can also display the much larger 20- to 150-mm wedge-shaped pulmonary parenchymal perfusion defects that result from the arterial occlusions[85]. Similarly, myocardial and intracranial perfusion defects are more readily identified at contrast-enhanced DECT than SECT. Reduced iodine dose at DECT angiography is also valuable to patients with aortic and peripheral vascular disease because such patients frequently have co-existing renal disease, as is the case in diabetics, patients with a history of smoking, and those with advanced atherosclerotic disease. Current DECT angiographic protocols that use reduced contrast material may require as little as half the contrast material dose required for SECT[86].

3.2. Improved lesion conspicuity

DECT enables improved disease detection by improving the conspicuity of lesions that otherwise have low contrast to surrounding organ parenchyma. For example, the detection of hypervascular liver lesions is critical for the diagnosis of hepatocellular carcinoma. These lesions may take up only slightly more iodinated contrast material compared to surrounding liver parenchyma. Use of iodine density images or virtual mono-energetic low-keV images allows one to amplify the iodine signal and improve the sensitivity of scans for these tumors (Fig. 8). Conversely, lesions that are slightly hypovascular to that of the surrounding organ parenchyma, such as pancreatic adenocarcinomas or hypovascular liver masses, may become more conspicuous since the organ parenchymal signal may be emphasized at DECT.

A substantial benefit of DECT is to reduce radiation dose by potentially obviating the need for an unenhanced CT scan that is frequently needed as a baseline to assess lesion enhancement by intravascular iodinated contrast material. For example, lesions in the kidney that show moderately high CT attenuation on a contrast-enhanced SECT scan are often ambiguous for malignancy versus a benign hyperdense cyst. If the lesion shows enhancement by iodinated contrast material, it is more than 85% likely to represent a malignancy[87]. If, instead, the lesion has intrinsic high CT attenuation and does not take up iodinated contrast material, then it is a benign cyst and does not require further evaluation or follow-up (Fig. 9). The unenhanced SECT scan is valuable to provide a baseline in order to evaluate for potential increase in contrast-enhanced attenuation; a substantial increase in contrast enhancement in a lesion compared to surrounding parenchyma would indicate vascularity and potential tumor tissue. However, the extra unenhanced CT scan doubles the radiation dose required to characterize the lesion properly. Unlike SECT scans, the images from DECT exams can be analyzed with material decomposition to generate both virtual unenhanced images and iodine density maps to determine whether or not iodinated contrast

enhancement is present, indicating tumor, or not present, which indicates a benign cyst – the need for an unenhanced CT scan is frequently not needed.

Dual-energy CT can also distinguish iodinated contrast material from other radiodense material. Radiodense calcified material commonly can be confused with enhancement by contrast material at SECT imaging. At DECT, this pitfall is mitigated because the signal of calcium may be distinguished from that of iodine by material decomposition. Currently, separation of the iodine signal from the calcium signal is less robust than from soft tissue signal, because the LACs of calcium and iodine are nearly identical at some concentrations, whereas the LACs of these elements at concentrations found in CT scans are generally very different from the LACs of soft tissues. Nevertheless, this separation is clinically valuable, for example to distinguish calcified vascular plaque from iodine-contrast enhanced vascular lumen at DECT. With DECT, active extravasation of iodinated agents can be differentiated from pre-existing calcifications that may mimic active bleeding at SECT. Virtual unenhanced CT images allow determination of contrast material enhancement versus unenhanced but highly attenuating soft tissue, or to characterize tissues for fat content without the need for a separate unenhanced CT scan.

3.3. DECT using multiple contrast agents

While current clinical CT imaging is of high value, certain prominent limitations remain. These limitations include the fact that, at SECT, different contrast materials introduced into different body compartments are not distinguishable from each other except by anatomic context alone. For example, enteric contrast material in the bowel lumen prevents evaluation of bowel wall vascular enhancement at SECT because the vascular and enteric contrast material may show similar signal (Fig. 10). Also, to perform a multiphase exam, such as for evaluation of liver, pancreatic, or renal lesions, repeated SECT scans need to be obtained as contrast material redistributes from the arteries to the organ parenchyma, to the veins, and then to the excretory systems. Multiphase exams result in high radiation doses to patients and separate image acquisitions are difficult to co-register with one another due to differences in breath-hold depth and the pulsation, rotation, and peristalsis of viscera between scans.

Several groups have demonstrated the possibility of simultaneous administration of two or more contrast materials with different reporter elements at DECT to exploit the ability of material decomposition to create separate material density maps for each contrast material. Initial studies were performed in a colon phantom and showed excellent separation of bismuth enteric contrast material from iodinated contrast material on a commercial dual-source DECT scanner[88]. A subsequent series of experiments by a different group in rodents showed the feasibility to deliver simultaneous bismuth enteric contrast and intravenous contrast material to provide high-spatial-resolution co-registered images of the bowel lumen and vasculature with a single DECT scan[19]. This group also showed that injection of a tungsten cluster contrast agent, followed by intravenous injection of iodinated contrast material, allowed for a single DECT scan to provide an arterial phase CT angiogram with the iodinated agent as well as a concurrent portal venous phase CT with the composite contrast materials. Staggered contrast material delivery for a single CT scan, rather than

staggered scan delays with a single contrast agent injection, effectively cut the radiation dose in half for a dual-phase arterial and venous phase exam, and also provided excellent image co-registration of the arterial and venous anatomy[19]. Another study using enteric bismuth and intravenous iodinated contrast agents at rapid-kVp-switching DECT was performed on rabbits with sharp penetrating abdominal trauma. This study showed that the accuracy of DECT was higher than that of conventional CT for determining whether contrast material leakage was from bowel perforation versus bleeding, and the addition of DECT allowed radiologists in training (residents) to perform as well or better than experienced trauma radiologists at this task[18].

Additional rabbit studies were performed to assess the image quality of scans of the bowel, obtained with conventional CT versus a DECT scans with tungsten, tantalum, or bismuth enteric contrast material and intravenous iodinated contrast material. These three enteric contrast agents provided excellent positive opacification of the bowel lumen, and DECT allowed for the subtraction of the enteric signal to allow visualization of the iodine vascular contrast material signal in the capillary beds of the bowel wall. In this study, subtraction of the tungsten and tantalum enteric contrast material from the iodine signal was excellent, while bismuth enteric contrast, which showed greater difference in the 80 to 140 kVp X-ray attenuation, showed poorer subtraction. In general, reporter elements that are more easily separated from each other by material decomposition are those with greater differences in their relative X-ray attenuations when imaged at low- versus high-kVp settings (Fig. 11)[43].

Dual-energy micro-CT at 40 and 80 kVp allowed the signal from intravascular iodinated contrast agent in the liposomal blood pool to be separated from that of gold nanoparticles that had passively accumulated into sarcoma tissue[89] or into lung tumors[21]. Using a prototype photon-counting, energy-discriminating CT system with four detector energy bins, another study showed that iodine and barium contrast material could be separated in a mouse carcass embedded in resin, despite the fact that iodine’s and barium’s K-edge energies are only 4 keV apart[90].

Future contrast material development could focus on agents that opacify different compartments of anatomy and which have low-mean-energy to high-mean-energy X-ray attenuation properties that are complementary to currently-available intravascular iodinated and enteric iodine- and barium-based agents. Examples of agents with different biodistribution include those that primarily distribute in the blood pool, in the hepatobiliary system, the reticuloendothelial system, the pulmonary airways, or that target specific tissues.

3.4. Targeted versus general agents

Currently no truly targeted contrast materials have been approved for CT imaging. A particular problem with the development of targeted agents for CT is the relatively poor sensitivity of CT for the detection of contrast materials. A concentration of approximately 2 mg of reporter element per cm^3 tissue is required for confident visualization of contrast materials at CT imaging. While DECT could reduce this requirement to approximately 1 mg/cm^3, the need to achieve high concentrations of retained reporter elements at target sites remains challenging from both practical and safety standpoints.

To address this challenge, targeted CT contrast agents must utilize strategies that allow a large amount of reporter element to bind to the target sites. Examples of described approaches include 1) branched polymeric structures that incorporate many atoms of the reporter elements into each molecule [91]; and 2) nanoparticles or liposomes [92] which allow for dense packing of the reporter element within a shell bound to ligands (Fig. 12)[93, 94]; and 3) the targeting of molecules that are present in high concentrations in the tissue of interest.

Despite the challenges to develop targeted CT agents, many preclinical examples have been described and summarized in prior reviews[95]. More recent examples include silica-coated ytterbium nanoparticles bound to calcium chelators which bind to damaged bone[96]. Unfortunately, most of these targeted agents are far from being practical for clinical translation and are limited mostly to preclinical research.

Clinical contrast materials currently in use that can be loosely considered to be targeted agents include the hepatobiliary contrast materials which show delayed uptake by hepatocytes and partial excretion via the biliary system[97]. A second class of contrast materials that could be considered semi-targeted are the oil-based agents, such as ethiodized oil, which may be delivered locally via transarterial chemoembolization to liver tumors. Ethiodized oil undergoes macrophage elimination in normal liver tissue, but shows prolonged retention in tumor tissues which lack macrophages[98].

Potentially translatable contrast materials include contrast material that may provide blood pool distribution, such as liposomal nanocarriers of existing iodinated agents which were in clinical phase 2 trials (NCTX™, Marval Pharma), perfluorooctylbromide emulsions[99], dendrimers, and biodegradable macromolecular agents[100]. Along with blood pool imaging, these agents enhance the reticuloendothelial system, and may show passive targeting of tissues with that show relatively high permeability of tumor microvessels to macromolecules[101].

4. Choice of elements for spectral CT contrast material

4.1. Critical considerations

The few contrast materials that dominate in CT usage today were not initially developed specifically for CT. Rather, these agents were initially developed as safe agents for fluoroscopic and plain-film radiography, and then later adopted for use with CT. With few exceptions, each of the agents shows similar enhancement at CT imaging. Now that DECT is available and can potentially distinguish between different “colors” (energy-dependent attenuation characteristics) of contrast agents, it is reasonable to revisit the periodic table to identify high-value reporter elements that could be developed into valuable clinical spectral-CT contrast materials. Future research on contrast materials for spectral CT benefits from the rich history of publications on potential non-iodinated X-ray contrast materials[102].

From a patient safety perspective, an ideal contrast agent must contain elements that are non-toxic, are formulated with physicochemical properties (viscosity and osmolality) that are compatible with high-concentration delivery into the body, and are cleared from the body

in a short time, i.e., a large fraction of the intravenously delivered material must be renally excreted in a timeframe of minutes to hours. For targeted agents, off-target binding must be very low, in light of the large amounts of agent (and requisite high target to background ratio) that needs to be present to be visible at CT imaging.

From a practical perspective, the elements used in general-purpose CT contrast agents must be available in large quantities and at low cost. Given that there are upwards of 40 million intravenous contrast-enhanced CT exams performed each year in the U.S. alone, and each exam requires approximately 30 grams of the contrast-producing element, over 1000 tons of that element would be required to meet the total annual U.S. demand, at a maximum raw materials price of a few dollars per 30 g dose. The global demand for material to produce contrast agents for CT can be estimated to be approximately 3,000 tons per year, assuming 30 g/CT scan and 90 million contrast-enhanced CT scans/year word wide. However, it is highly likely that iodinated agents will continue to meet at least two-thirds of that demand, even with the introduction of new agents based on high-Z elements. Therefore, we will consider the requirement to be approximately 1,000 tons of the required element annually. Of course, the use of that element for contrast agents should only be a fraction of the global production, but if there is increased demand, we would anticipate that production would increase in order to meet the demand, if sufficient reserves are available.

From an imaging efficacy perspective, an ideal element for use as a conventional CT contrast agent would be one that provides high image contrast (i.e., high contrast-enhanced HU compared to soft-tissue HU) on a per-mass-concentration basis. To best complement the existing iodine- and barium-based contrast agents, which have large differences in HU when imaged at low- versus high-kVp settings, excellent DECT agents would have dramatically different attenuation properties than these agents across the kVp settings used for clinical imaging, for example, having a constant HU across the kVp settings. Similarly, the ideal material would be one that has a substantial difference in HU compared to calcium, which is commonly seen in atherosclerotic plaques, bone, or diseased tissues. Because the CT number of calcium decreases with increasing kVp settings, an excellent contrast material for use near calcified structures would have constant or increasing HU with increasing kVp. The primary physical X-ray attenuation mechanism that produces differentiated HU as a function of photon energy is the K-edge energy of the contrast-producing element. If there are multiple contrast-producing elements in the contrast agent, the overall kVp-dependent HU depends on the weighted effects of the K-edge energies of the contrast-producing elements in the contrast agent.

We can evaluate the potential applicability of each element for use as a CT contrast agent by reviewing the periodic table (Fig. 13) and some basic characteristics of the candidate elements[103–106] summarized in Table 1.

Iodine (shown in light green background in Fig. 13 and Table 1) is currently the only element used as an intravascular (IV) contrast agent at CT. Iodine is particularly efficacious when imaged at lower-kVp settings (i.e. 70 kVp – 100 kVp), such as for children and small- to medium-sized adults. However, the X-ray attenuation of iodine diminishes rapidly at higher-kVp settings required to image large sized body parts; therefore, large contrast

material doses are needed to maintain a similar contrast-to-noise ratio at high-kVp settings. Use of higher atomic number (higher-Z) elements which do not lose as much X-ray attenuation at higher-kVp settings may allow for improved imaging at high-energy spectra without increased contrast material dose. Furthermore, within the diagnostic X-ray energy range, iodine's and calcium's similar MACs both monotonically decrease with increasing energy, limit the accuracy of distinguishing iodine contrast material from calcium at spectral CT. Higher-Z elements could improve the ability to distinguish contrast agents from calcium at spectral CT.

All elements with atomic numbers (Z) below that of iodine (Z=53) are marked in brown and are excluded from further consideration because they would produce even lower HU than iodine, and therefore would offer no advantage.

We can eliminate (marked in red) gases, known toxins, radioactive elements, and synthesized elements.

All elements between Z=75 (Rhenium) and Z=79 (gold) are impractical for general-purpose agents (marked in orange) because they are either produced in minimal quantity or cost far more than practical for a general-purpose contrast agent (see Table 1). Of these, gold is marked with a dark green background because it may have some potential niche applications in medical imaging and radiation therapy. Nevertheless, targeted agents could potentially use more expensive elements.

A number of elements (shown in black and white) are worthy of consideration as the basis for contrast materials because they show efficient X-ray attenuation at CT. However, the total annual production of many of these, particularly Z=62 (samarium) through Z=72 (hafnium), is currently too small to satisfy the market need for the active element in a general-purpose contrast agent. On the other hand, those in the range of Z=57 (lanthanum) through Z=60 (neodymium) are produced in sufficient quantity at low-enough cost to at least partially satisfy the market demand for a general purpose contrast agent. Furthermore, these elements would provide CT image contrast that would be a substantial improvement over iodine; therefore these are worthy of further investigation.

All elements that are marked with a green background are either currently in use as contrast agents, or have been reported in the literature as potential candidates for new contrast agents. These are discussed in more detail in the next section.

There are two main reasons to develop new clinical CT contrast agents. The first reason is to provide some technical or image quality advantage over the current iodinated agents. The technical disadvantages of iodinated agents have been described in previous sections. The second reason would be to offer an improved or substantially different safety profile that would benefit patients with poor renal function or history of reactions to iodinated agents. An ideal contrast agent might satisfy both properties, but safety will always be of paramount importance. In the following sections we review key elements that have been studied for CT and X-ray imaging and that show promise as spectral CT contrast agents. Several excellent review articles have been published on radio-opaque agents especially with nanoparticle constructs[107–112]. Several recent academic papers have shown the potential for

multimodal use; such studies would include theranostic agents which provide a combination of diagnostic and therapeutic functions[113].

We note that the majority of the X-ray contrast agents based on the elements discussed in the following sections have not been evaluated comprehensively (or at all) for biocompatibility and safety at the dose required for CT contrast agents, nor have they been rigorously evaluated for CT imaging efficacy. Notable exceptions are iodine, which has been extensively developed and studied and is in current use as an IV-injected agent, barium, which has also been in long use as an orally-administered CT contrast agent; gadolinium, which is in use as an IV-injected MR contrast agent and has in the past been used off-label at CT; tantalum, which among experimental agents in the literature, has been reported the most comprehensively as a potential element for use in a general-purpose nanoparticle-based CT contrast agent; and gold, which has been reported even more comprehensively, but due to cost considerations, is practical as an element for use only as a niche-application nanoparticle-based CT contrast agent.

Furthermore, we note that among the experimental nanoparticle-based agents that have been reported, most are large nanoparticles (tens or even hundreds of nanometers), and therefore clearance times are long and via the liver; very few are in the size range required for fast renal clearance (approximately 3–4 nm or smaller) and of those, there have been almost no rigorous safety studies reported.

In many articles that explore the use of experimental elements for X-ray contrast agents, in vitro (phantom) and in vivo (small animal) imaging results are shown. While these reports confirm that the imaged elements do attenuate X rays, the results should be interpreted with some caution for a number of reasons. First, the mass concentration of the active element and the composition of the solvent that is used are often unspecified and/or uncontrolled, and may not be realistic for clinical use. Second, the imaging conditions are often unspecified or not clinically relevant. In particular, as described in section 2, the X-ray spectrum is a critical factor in the resulting image quality and so the kVp needs to be similar to that of a clinical CT scanner. Furthermore, the subject size plays an important role in shaping the spectrum. Other concerns related to experimental design include vial size and measurements statistics for in vivo studies, and biological safety and clearance mechanism for *in vivo* studies. The authors encourage the reader to explore the literature with interest, and to consider these and other concerns when evaluating the potential clinical feasibility of a given material.

4.2. Main group elements

Elements drawn from the non-lanthanide, non-transition metals portion of the periodic table are considered first, because they include the most commonly used clinical contrast reporter elements, iodine and barium.

4.2.1. Iodine/Barium—Iodine (Z=53) is the only element approved for intravascular (IV) administration for X-ray/CT scans. These agents are almost universally based on a tri-iodinated benzene ring with additional substituents to confer the desirable properties of safety, viscosity and osmolality. Iodinated agents have an excellent safety record[114, 115]

but small subsets of patients may be susceptible to injury[116]. Dimeric agents were developed in order to produce potentially safer iso-osmolar agents and more recent studies have focused on producing more physiological formulations through lowering viscosity or the addition of electrolytes to hexaiodinated compounds[117–120].

Since the available iodinated contrast agents are relatively small molecules approximately 1.3 – 2.1 nm in size[121], a variety of strategies have been developed to generate longer-circulating materials as blood-pool agents (agents that reside in the vasculature for longer periods of time)[122]. These include polymeric constructs[100, 123] (including dendrimers[124]), emulsions[125, 126], micelles[127], liposomes[122] and nanoparticles[128–130] One variant employs a liposomal iodinated agent for high-resolution imaging with a blood pool contrast agent[131]. A coated version of polymeric iohexol has also been employed to exploit the longer retention in the body[129]. The biodistribution of iodinated agents is sensitive to specific chemical constructs; iodinated monoglycerides exhibited significant uptake in the liver (17% of dose) at 24 h, followed by a decline; whereas iodinated vitamin E climbed to almost 80% in the liver with very slow elimination kinetics[126].

Barium (Z=56) has been used primarily as an oral agent with a focus on delineating the bowel lumen. The specific compound is usually barium sulfate, which is an inert nano- or microparticle. Barium sulfate has been used clinically for over 50 years, and US FDA new drug application clearance was obtained in 2016. Barium is used cautiously in cases of potential bowel perforation because leakage of the agent outside of the intestines may cause or worsen inflammation. There has been interest in investigating barium as one component of a multiple-agent contrast-enhanced DECT exam protocol to improve diagnostic capability[132, 133]. Barium sulfate nanoparticles have also been prepared for animal research[134]. Another paper reported the synthesis of barium carbonate nanoparticles coated with D-glucuronic acid which were imaged in mice[135]. A number of examples of combinations of barium in conjunction with rare earth elements have been reported such as $BaYbF_5$[136, 137] and $BaHoF_5$[138].

4.2.2. Xenon—Xenon (Z=54) is a noble gas between iodine and barium in the periodic table, and as such it has a similar LAC to these elements; however, because xenon is a gas and cannot be administered by IV injection, it is difficult to compare with iodine and barium. Furthermore, gaseous xenon has a low density; therefore, its MAC as a gas is much lower than those of iodine and barium. Although xenon does not have US FDA approval, it has been explored as an inhalational agent that dissolves into blood for human patients in a number of applications[111]. Some recent explorations on xenon studied blood flow[139] and neurochemistry[140]. Xenon has been shown in several studies as an effective dual-energy inhalational contrast material to reveal pulmonary ventillation abnormalities[141, 142]. Potentially, xenon could be used in conjunction with other complementary agents at spectral CT for multiple-agent contrast-enhanced scans.

4.2.3. Gallium—Gallium (Z=31) is a metal, but liquid gallium has been reported for use in X-ray imaging of vascular networks for *in vitro* depiction of organ anatomy and was suggested for use *in vivo* under localized conditions[143]. However, the very low atomic

number of gallium results in an inefficient X-ray attenuation that is substantially lower than that of iodine.

4.2.4. Bismuth—Bismuth (Z=83) has been used for over 100 years as an over-the-counter remedy for gastrointestinal problems[144]. Bismuth has the highest K-edge energy (91 keV) of all the elements under consideration and as a result, it shows less change in CT number across different kVp settings compared to iodine and barium. Bismuth sulfide is inert and has been described as a nanoparticle contrast agent[145]. Platelets of Bi_2S_3 were coated with polyvinylpyrrolidone (PVP) and imaged both *in vitro* and *in vivo*; the authors stressed the importance of the PVP coating for biocompatibility. More recent work with bismuth sulfide has considered Pluronic coatings[146] and dendrimer stabilization[147]. A targeted bismuth sulfide nanoparticle was generated with a label for breast cancer in mice[148]. Sailor and co-workers showed a significant increase in contrast agent uptake in tumors using the labeled nanoparticles (8% compared to 3% of injected dose) but there were clearance issues with substantial retention in the spleen. Other researchers have explored bismuth oxide[149], bismuth oxychloride[150] and even elemental bismuth[151] as core materials for contrast agents. Another example use of bismuth employs a molecular species, bismuth decanoate, that is ultimately encapsulated by phospholipids[152]. These authors exploited the K-edge energy of bismuth to more clearly differentiate contrast agent from calcium than could be obtained using traditional contrast agents. Bismuth suspensions were employed in a similar manner for studies at DECT directed toward metal artifact reduction[133].

In multi-modality imaging (i.e., use of more than one imaging modality with the same contrast agent), FeBi nanoparticles that were visible at both MRI and CT imaging have been described[153, 154]. Similarly, MRI and CT can be used to visualize nanoparticles synthesized using bismuth surfactants in the precipitation of iron oxide[155]. Silica-coated bismuth sufide nanorods were shown to provide image contrast enhancement at CT imaging and also provide enhancement at photoacoustic tomography[156].

4.3. Transition metal elements

4.3.1. Lutetium—Lutetium (Z=71) appeared in a recent publication employing PEGylated nanoparticles[157]. Another paper has reported the use of PEGylated $NaLuF_4$ which allows for the combination of fluorescence and X-ray imaging[158].

4.3.2. Tantalum—The oxide form of tantalum (Z=73), Ta_2O_5, is chemically inert[159], biocompatible[160], and shows good radiopacity[161] as evidenced by historic use as a water-insoluble powder for tracheobronchial[162, 163] and gastrointestinal[164, 165] imaging. In recent years, nanoparticles of tantalum oxide have been synthesized and formulated with coatings to permit intravenous injection for imaging. One formulation of tantalum oxide nanoparticles used organofunctional siloxane-based coatings[166–168] to impart biocompatibility and promote renal clearance, while others followed with PEGylated coatings on larger nanoparticles[169, 170].

Some authors of this review have worked to develop a new nanoparticle-based general-purpose contrast agent that could be concentrated (240–320 mg Ta/mL) and formulated to be iso-osmolar with blood (~290 mOsm/kg) while maintaining low viscosity (~5–7 mPa s at

37°C). It was thought an agent featuring these physicochemical properties would be a reasonable solution for a vascular imaging agent, with tantalum serving as a novel reporter element to enable new imaging applications and advantages over currently-available iodinated contrast media. While initial endeavors with coatings derived from either PEG[171] or phosphonate esters[166] yielded highly viscous solutions at moderate tantalum concentrations (≤190 mg Ta/mL), more recent zwitterionic forms of tantalum oxide nanoparticles were found to dramatically reduce viscosity of concentrated solutions, significantly decrease tissue retention of injected tantalum in rat dosing studies, and eliminate a pathological response in rat kidneys previously observed with a coating derived from a phosphonate ester[167, 172].

In 2015, a single-ligand (intramolecular) zwitterion-coated tantalum oxide nanoparticle was shown to have a very promising safety profile at an anticipated clinical dose of 400 mg Ta/kg[172]and retention was found to be comparable to that of a clinical iodinated contrast agent as observed in rat dosing studies[11, 118, 173]. A recent report shows that a contrast agent based on these zwitterionic-coated tantalum-oxide nanoparticles has CT imaging performance that exceeds that of an iodinated agent, and exhibits the best physiochemical, clearance, and safety profiles compared to any proposed new contrast agent in the literature[121]. Therefore, these experimental agents show promise as the next generation of clinical intravascular contrast agents.

In other work, tantalum oxide nanoparticles have been encapsulated into polypyrrole as a composite and used for CT/photoacoustic imaging-guided photothermal ablation of tumors[174]. Small molecule cluster compounds of tantalum have been proposed as contrast agents based on increased X-ray attenuation properties of clusters compared to iodinated contrast agents, however to date these formulations lack biocompatibility[161, 175].

4.3.3. Tungsten—Adjacent to tantalum in the periodic table, tungsten (Z=74) would be expected to provide similar performance as a contrast element. One recent example employs polymer-coated tungsten-oxide nanoparticles[176]. An alternative coating of poly(ethylene glycol) has been studied for both imaging and photothermal therapy[177, 178]. Sodium tungstate nanoparticles coated with D-glucuronic acid have been reported and imaged[135]. Manganese tungstate has been used as a multi-modality agent – useful both for CT and MRI imaging[179]. Studies also include tungsten as an agent with potentially useful characteristics for advanced methodologies[19, 133] such as at DECT for metal artifact reduction.

4.4. Coinage metals

4.4.1. Gold—Gold (Z=79) has a rich history in nanomaterials development dating at least to Roman times with the use of gold colloids for dyes[180]. Since then, an extensive chemistry has developed related to gold nanoparticles, including various bio-applications such as CT imaging[181]. There are probably more publications about gold nanoparticles than there are about all the rest of the elements combined. A recent review was entirely devoted to gold nanoparticles as contrast agents[182]. Although the high price of gold may make it impractical for use as a general-purpose intravascular contrast agent, there certainly

may be specific applications for which the use of gold is potentially cost effective, for example as targeted contrast agents for oncology, or for theranostic contrast agents. Moreover, key knowledge developed from investigation of gold nanoparticles may be transferred to other elements, such as the formulation of coating modifications, and bioconjugation.

The concept of gold nanoparticles as X-ray contrast material dates back at least to 2004[181, 183]. There are several advantages of gold as an active element in a contrast agent. Gold is known to be relatively inert and it is possible to make the core comprised totally of gold atoms such that the mass concentration of gold in the nanoparticle is very high. Such properties allow for the preparation of concentrated gold solutions that have low viscosity and low osmolality. However, the mass-concentration-normalized CT X-ray attenuation of gold is below that of every other element that was considered in a fairly comprehensive study[106] ; to some extent this offsets the benefit of the high mass concentration that can be achieved in gold nanoparticles.

A group of articles have appeared which combine gold nanoparticles in a dendrimer framework[184–188]. One potential advantage of this strategy is to bring multiple nanoparticles to a target such as a carcinoma by modification of the dendrimer with a targeting moiety.

Recent work has demonstrated a variety of materials that have multi-modal capability. One example uses gold nanoparticles modified by silica to enable both CT and fluorescence imaging[189]. Another paper used gold nanoparticles with both X-ray and fluorescent imaging for brain gliomas[190]. Yet another example combines MRI with CT imaging by synthesis of a composite structure with both gadolinium and gold[191].

4.4.2. Silver—Silver (Z=47), which has lower Z- and K-edge energies than iodine, has been explored in a modest number of publications as a reporter element for CT. One publication suggests that silver may have advantages in dual-energy X-ray mammography[192]. Another study prepared a contrast agent from 9- to 23-nm nanoparticles of silver stabilized with dendrimers which was then compared with iodine-based agents[193]. One group considered taking advantage of the anti-bacterial properties of silver nanoparticles while also imaging at CT for inner ear applications[194].

4.5. Lanthanide elements

The atomic numbers of lanthanides range from Z = 57 to 71 and these elements have slightly higher K-edge energies than do iodine and barium. The lanthanides have been explored as potential imaging agents, though there has been more attention to MRI and optical imaging than CT[195]. The chemistry of these elements is dominated by oxidation state III, so for example the oxides would be La_2O_3.

4.5.1. Gadolinium—Gadolinium (Z=64) compounds have been used extensively as MRI agents[196] typically as complex chelates. While earlier work used the MRI agents at elevated doses[197], more recent work has considered a variety of nanomaterials[191, 198–200]. One example employed PEGylated gadolinium hydroxide nanorods[201]. A number of

studies have included gadolinium as part of a multi-modal agent; these include PEG-modified $BaGdYF_5$[202] and a europium doped gadolinium oxide[199]. Since approximately 40 times higher dose of gadolinium is needed for effective contrast enhancement at CT imaging than for MR imaging, potential safety concerns are prominent when considering gadolinium agents for CT. These concerns include possible nephrogenic systemic fibrosis in patients with severe renal insufficiency, and recent findings that gadolinium may be retained in the brain and bones of patients following gadolinium contrast-enhanced MR imaging[203–205].

4.5.2. Ytterbium—Using ytterbium (Z=70), one study specifically designed to take advantage of spectral CT imaging used a trivalent ytterbium complex as the core of a nanocolloid[206]. Pan and coworkers determined in a mouse model that approximately 90% of the injected dose showed bioelimination within seven days, with most of the remaining ytterbium found in the liver. A variety of ytterbium-based contrast materials have been considered [202, 207–209], many designed for multimodal diagnostic capabilities. One example contrast material designed for both CT and fluorescent imaging showed approximately 75% bioelimination within a week and concentrations reduced to near the level of detectability within 30 days[209].

5. General biological and regulatory hurdles

No substantially novel radiographic contrast agents have been approved in over 20 years. This is due, in part, to the many challenges of shepherding a new agent through the regulatory approval process, which is generally governed by the same regulations that apply to standard therapeutic pharmaceuticals. In particular, existing imaging contrast agents show very low risk for substantial injury[12, 210]. To be efficacious as a new rapidly-eliminated intravenous CT contrast material, very high single doses of the new material must be safe for rapid administration to produce relatively high concentrations in the body at the time of imaging; the dose requirement is on the order of 30 g of the active element for a typical adult; the dose is typically injected intravenously in approximately 10–30 seconds. Alternatively, slowly eliminated contrast materials such as blood pool or targeted agents must demonstrate a high safety profile despite prolonged exposure to the substantial quantity of material required to be visible at CT. Therefore, the safety requirements for new CT contrast materials are very demanding.

Magnetic resonance imaging and ultrasound contrast media are used at doses of ~30 mg/kg bodyweight (BW) and ~1 mg/kg BW, respectively. CT contrast media, in comparison, are used at doses beginning at ~100 mg/kg BW, and are frequently used at substantially higher doses up to approximately 2000 mg/kg BW. The impact of these required doses on the process of ensuring the safety of the drug is profound. In addition to routine toxicological considerations, contrast agents administered at such high doses may have an impact on clearance organs[211]. Rapid and complete clearance of contrast agents is conceptually related to preferable safety profiles. Low residence time equates to limited total systemic exposure. Paradoxically, low residence time also creates an increased burden on the clearance organs, usually the kidneys.

As for a standard pharmaceutical, any putative new CT contrast material will have to undergo routine safety toxicological testing at higher doses than used in the clinical setting. Nonclinical safety studies required for the registration of new pharmaceuticals, including contrast media, usually involve the administration of doses to animals that are orders of magnitude above the efficacious clinical dose. This testing is intended to determine the dose at which adverse effects, defined as any effect that would be unacceptable in the clinical setting, occur in animal models (usually in two species, one rodent and one non-rodent). The highest doses tested without adverse effects (termed the no-observed-adverse-effect-level, NOAEL) is then compared with the maximum intended clinical dose to give a margin of safety, which accounts for potential uncertainty related to species differences and variation between individual patients. For standard pharmaceuticals, this is often on the order of 10 to 100 times the clinical intended dose. The challenge with CT contrast media relates to the very high doses used in the clinic. Since contrast media are often formulated at near to their limit of solubility and there are volume limitations recommended for the administration of substances to laboratory animals[212], there is a limit to the maximum dose that is possible to test in animals (termed the maximum feasible dose, MFD). When this maximum feasible dose is compared with the high doses used clinically, margins of safety can often be less than 10. When evaluating potential iodine-based agents, trial designs can somewhat compensate for this limitation by relying on comparison to historical safety data from the drug class, which is well established and understood. A hurdle for novel molecular entities is the absence of historical knowledge to help guide their development and focus on specific risks. As an example, a liposomal agent based on iodine showed no adverse effects at 10–30 mg I/kg, but there were issues at 70–100 mg I/kg in a phase-I clinical trial[213]. Lack of historical data raises the burden of proof required to demonstrate safety. Understanding the biodistribution and clearance of the novel contrast materials within the body helps focus safety trials on the most relevant endpoints.

The required rapid rate of administration of CT contrast materials presents a second physiological challenge for the development of novel agents. In order to achieve the concentrations necessary to effectively attenuate X rays, the concentrations of injected contrast material generally need to be in the hundreds of mg active element / mL of solution. To provide sufficient concentrations in the target anatomy, especially in vascular applications, CT contrast materials are administered at very high rates (e.g. 5 mL/second) for a high total volume (e.g. 100 mL) using a power injector. The high concentrations of such agents generally mean that solutions are often hyperosmolar with respect to blood, as well as being more viscous than blood. The combination of the physicochemical characteristics of a contrast agent solution and the high rate of administration brings with it a host of potential adverse physiological responses. Patients can often feel pain at the site of injection and generalized nausea with rapid injection of contrast media having a substantially higher osmolality than blood. Anaphylactoid reactions may also occur with histamine release via a poorly understood pathway[214]. In addition, X-ray contrast media are commonly injected directly into arteries, such as the coronary arteries during interventional angiographic procedures. Such injections expose target organs, such as the heart, to extremely high local concentrations of contrast material. A more physiologically-compatible formulation is particularly desirable for such applications to limit potential side effects on heart function.

One advantage of currently available contrast materials is that, after numerous iterations on the common tri-iodobenzene motif, contrast materials have been identified that have relatively low viscosity and low osmolality. Some agents are iso-osmolar with blood, even at concentrations in excess of 600 mg/mL. In order to be a viable clinical candidate, any new general-purpose CT contrast agent must meet or at least approach these physicochemical parameters. Unfortunately, many experimental compounds that provide excellent opacification at CT fail to meet the required physicochemical requirements when concentrated to clinically-useful levels. The solubility required to make sufficiently-concentrated solutions are often a challenge as well, as many promising compounds are not soluble to the desired degree.

Finally, among the most daunting regulatory obstacles for new contrast materials are the contrast agents that already exist. The current agents, all of which are based on the common tri-iodobenzene core, either in monomeric or dimeric form, are incredibly safe. Since the tri-iodobenzene ring was first introduced over 50 years ago, the manufacturers of these agents have successively improved the hydrophilic substituents onthe contrast-generating core to reduce toxicity. The current agents are well-tolerated and inexpensive, with known safety profiles and relatively low risk of adverse events. In order to be considered for widespread use, a new agent would need to meet or improve upon these existing safety profiles at the very high doses discussed above, and also provide evidence of some benefit in contrast enhancement or performance. Of note, CT contrast agents are used in patients with a wide range of disease, meaning that their required safety profile is more rigorous than might otherwise be the case. Unlike specialized therapeutic agents which may be permitted to have some degree of toxicity if their therapeutic benefit is large, general-purpose diagnostic contrast material must be extremely safe in order to be accepted clinically. Potential approaches to mitigate safety concerns include developing contrast agents for delivery into less sensitive bodily compartments, such as the bowel or bladder, or developing targeted agents that may be given at lower doses than would a general agent. However, the market for such specialized agents is substantially smaller than for more general agents and the commercial development of any new agent requires careful consideration of economic feasibility.

In summary, the regulatory challenges for any new contrast material are in part due to the large mass concentration needed to attenuate X-rays, and in part due to the mature nature of the current generation of agents. However, the possibility of spectrally active contrast material – those whose active contrast-enhancing elements can interact specifically with X-rays in the CT energy range – may change the balance of the cost-benefit equation for new agents; spectrally active contrast material may enable rapid and more specific clinical diagnoses with lower radiation dose to patients. Agents that could have such profound impact on patient outcomes may justify the long and difficult process required to develop and certify a new agent.

6. Summary

Clinical CT scanners now commonly provide dual-energy capability that can increase the sensitivity to existing iodine- and barium-based contrast material and also can differentiate

these agents from other radiopaque materials. This latter capability of spectral CT has created the opportunity to develop new non-iodine-based contrast materials that differ in X-ray attenuation properties from current clinical contrast agents. Thoughtfully designed contrast materials that exploit untapped capabilities of spectral CT may introduce profound diagnostic advantages at spectral CT and therefore may be worth long-term investment. Given the established history of proven safety and efficacy of current X-ray contrast materials, it is imperative that any new contrast material be thoroughly vetted to minimize patient risks and ensure its benefit to society.

Acknowledgments

This work was supported in part by NIH grant R01EB015476. The content is solely the responsibility of the authors and does not necessarily represent the official views of the NIH.

References

1. Consumer Reports, Dangers of Having Too Many CT Scans, in, 2014.
2. Novelline RA, Rhea JT, Bell T. Helical CT of abdominal trauma. Radiologic clinics of North America. 1999; 37:591–612. vi–vii. [PubMed: 10361548]
3. Pietryga JA, Morgan DE. Imaging preoperatively for pancreatic adenocarcinoma. Journal of gastrointestinal oncology. 2015; 6:343–357. [PubMed: 26261722]
4. Shuman WP, Chan KT, Busey JM, Mitsumori LM, Koprowicz KM. Dual-energy CT Aortography with 50% Reduced Iodine Dose Versus Single-energy CT Aortography with Standard Iodine Dose. Academic radiology. 2016; 23:611–618. [PubMed: 26897602]
5. Zhang LJ, Lu GM, Meinel FG, McQuiston AD, Ravenel JG, Schoepf UJ. Computed tomography of acute pulmonary embolism: state-of-the-art. European radiology. 2015; 25:2547–2557. [PubMed: 25773940]
6. Bae KT. Peak Contrast Enhancement in CT and MR Angiography: When Does It Occur and Why? Pharmacokinetic Study in a Porcine Model. Radiology. 2003; 227:809–816. [PubMed: 12702823]
7. Bae KT. Intravenous Contrast Medium Administration and Scan Timing at CT: Considerations and Approaches. Radiology. 2010; 256:32–61. [PubMed: 20574084]
8. Bae KT, Heiken JP, Brink JA. Aortic and hepatic peak enhancement at CT: effect of contrast medium injection rate--pharmacokinetic analysis and experimental porcine model. Radiology. 1998; 206:455–464. [PubMed: 9457200]
9. Chu LL, Joe BN, Westphalen AC, Webb EM, Coakley FV, Yeh BM. Patient-specific time to peak abdominal organ enhancement varies with time to peak aortic enhancement at MR imaging. Radiology. 2007; 245:779–787. [PubMed: 17911535]
10. Schneider JG, Wang ZJ, Wang W, Yee J, Fu Y, Yeh BM. Patient-tailored scan delay for multiphase liver CT: improved scan quality and lesion conspicuity with a novel timing bolus method. AJR American journal of roentgenology. 2014; 202:318–323. [PubMed: 24450671]
11. Heglund IF, Michelet AA, Blazak WF, Furuhama K, Holtz E. Preclinical pharmacokinetics and general toxicology of iodixanol. Acta radiologica Supplementum. 1995; 399:69–82. [PubMed: 8610532]
12. Katayama H, Yamaguchi K, Kozuka T, Takashima T, Seez P, Matsuura K. Adverse reactions to ionic and nonionic contrast media. A report from the Japanese Committee on the Safety of Contrast Media. Radiology. 1990; 175:621–628. [PubMed: 2343107]
13. Coursey CA, Nelson RC, Boll DT, Paulson EK, Ho LM, Neville AM, Marin D, Gupta RT, Schindera ST. Dual-Energy Multidetector CT: How Does It Work, What Can It Tell Us, and When Can We Use It in Abdominopelvic Imaging? Radiographics. 2010; 30:1037–1055. [PubMed: 20631367]

14. Coupal TM, Mallinson PI, Gershony SL, McLaughlin PD, Munk PL, Nicolaou S, Ouellette HA. Getting the Most From Your Dual-Energy Scanner: Recognizing, Reducing, and Eliminating Artifacts. AJR American journal of roentgenology. 2016; 206:119–128. [PubMed: 26700343]
15. Pessis E, Campagna R, Sverzut JM, Bach F, Rodallec M, Guerini H, Feydy A, Drape JL. Virtual monochromatic spectral imaging with fast kilovoltage switching: reduction of metal artifacts at CT. Radiographics : a review publication of the Radiological Society of North America, Inc. 2013; 33:573–583.
16. Winklhofer S, Lambert JW, Wang ZJ, Sun Y, Gould RG, Zagoria RJ, Yeh BM. Reduction of peristalsis-related gastrointestinal streak artifacts with dual-energy CT: a patient and phantom study. Abdominal radiology. 2016
17. Luo XF, Xie XQ, Cheng S, Yang Y, Yan J, Zhang H, Chai WM, Schmidt B, Yan FH. Dual-Energy CT for Patients Suspected of Having Liver Iron Overload: Can Virtual Iron Content Imaging Accurately Quantify Liver Iron Content? Radiology. 2015; 277:95–103. [PubMed: 25880263]
18. Mongan J, Rathnayake S, Fu Y, Gao DW, Yeh BM. Extravasated Contrast Material in Penetrating Abdominopelvic Trauma: Dual-Contrast Dual-Energy CT for Improved Diagnosis—Preliminary Results in an Animal Model. Radiology. 2013; 268:738–742. [PubMed: 23687174]
19. Mongan J, Rathnayake S, Fu Y, Wang R, Jones EF, Gao DW, Yeh BM. In Vivo Differentiation of Complementary Contrast Media at Dual-Energy CT. Radiology. 2012; 265:267–272. [PubMed: 22778447]
20. Rathnayake S, Mongan J, Torres AS, Colborn R, Gao DW, Yeh BM, Fu Y. In vivo comparison of tantalum, tungsten, and bismuth enteric contrast agents to complement intravenous iodine for double-contrast dual-energy CT of the bowel. Contrast media & molecular imaging. 2016
21. Ashton JR, Clark DP, Moding EJ, Ghaghada K, Kirsch DG, West JL, Badea CT. Dual-energy micro-CT functional imaging of primary lung cancer in mice using gold and iodine nanoparticle contrast agents: a validation study. PloS one. 2014; 9:e88129. [PubMed: 24520351]
22. Falt T, Soderberg M, Wasselius J, Leander P. Material Decomposition in Dual-Energy Computed Tomography Separates High-Z Elements From Iodine, Identifying Potential Contrast Media Tailored for Dual Contrast Medium Examinations. Journal of computer assisted tomography. 2015; 39:975–980. [PubMed: 26295191]
23. Kalra MK, Maher MM, Toth TL, Hamberg LM, Blake MA, Shepard JA, Saini S. Strategies for CT Radiation Dose Optimization. Radiology. 2004; 230:619–628. [PubMed: 14739312]
24. Dodge, CW. A rapid method for the simulation of filtered X-ray spectra in diagnostic imaging systems. Wayne State University; 2008.
25. Hubbell, JH., Seltzer, SM. Tables of X-Ray Mass Attenuation Coefficients and Mass Energy-Absorption Coefficients from 1 keV to 20 MeV for Elements Z = 1 to 92 and 48 Additional Substances of Dosimetric Interest. NIST; 1996.
26. Poole, DM. X-ray absorption edges, characteristic X-ray lines and fluorescence yields. 2005.
27. Hounsfield G. Computed medical imaging. Science. 1980; 210:22–28. [PubMed: 6997993]
28. Hounsfield GN. Computerized transverse axial scanning (tomography): Part 1. Description of system. Br J Radiol. 1973; 46:1016–1022. [PubMed: 4757352]
29. Genant HK, Boyd D. Quantitative bone mineral analysis using dual energy computed tomography. Invest Radiol. 1977; 12:545–551. [PubMed: 591258]
30. Brooks RA, Di Chiro G. Split-detector computed tomography: a preliminary report. Radiology. 1978; 126:255–257. [PubMed: 619422]
31. Chiro GD, Brooks RA, Kessler RM, Johnston GS, Jones AE, Herdt JR, Sheridan WT. Tissue signatures with dual-energy computed tomography. Radiology. 1979; 131:521–523. [PubMed: 441344]
32. Millner MR, McDavid WD, Waggener RG, Dennis MJ, Payne WH, Sank VJ. Extraction of information from CT scans at different energies. Med Phys. 1979; 6:70–71. [PubMed: 440238]
33. Alvarez RE, Macovski A. Energy-selective reconstructions in X-ray computerized tomography. Phys Med Biol. 1976; 21:733–744. [PubMed: 967922]
34. Avrin DE, Macovski A, Zatz LM. Clinical Application of Compton and Photo-Electric Reconstruction in Computed Tomography: Preliminary Results. Invest Radiol. 1978; 13:217–222. [PubMed: 711396]

35. Adams JE, Chen SZ, Adams PH, Isherwood I. Measurement of Trabecular Bone Mineral by Dual Energy Computed Tomography. J Comput Assisted Tomogr. 1982; 6:601–607.
36. Chapman RW, Williams G, Bydder G, Dick R, Sherlock S, Kreel L. Computed tomography for determining liver iron content in primary haemochromatosis. Br Med J. 1980; 280:440–442. [PubMed: 7370525]
37. Goldberg HI, Cann CE, Moss AA, Ohto M, Brito A, Federle M. Noninvasive quantitation of liver iron in dogs with hemochromatosis using dual-energy CT scanning. Invest Radiol. 1982; 17:375–380. [PubMed: 7129818]
38. Cann CE, Gamsu G, Birnberg FA, Webb WR. Quantification of calcium in solitary pulmonary nodules using single- and dual-energy CT. Radiology. 1982; 145:493–496. [PubMed: 7134457]
39. Beutel, J., Kundel, HL., Van Metter, RL. Handbook of Medical Imaging: Physics and psychophysics. SPIE Press; 2000.
40. Johnson TR. Dual-energy CT: general principles. AJR Am J Roentgenol. 2012; 199:S3–8. [PubMed: 23097165]
41. Gabbai M, Leichter I, Mahgerefteh S, Sosna J. Spectral material characterization with dual-energy CT: comparison of commercial and investigative technologies in phantoms. Acta Radiol. 2015; 56:960–969. [PubMed: 25182803]
42. Fält T, Söderberg M, Wassélius J, Leander P. Material Decomposition in Dual-Energy Computed Tomography Separates High-Z Elements From Iodine, Identifying Potential Contrast Media Tailored for Dual Contrast Medium Examinations. J Comput Assisted Tomogr. 2015; 39:975–980.
43. Rathnayake S, Mongan J, Torres AS, Colborn R, Gao DW, Yeh BM, Fu Y. In vivo comparison of tantalum, tungsten and bismuth enteric contrast agents to complement intravenous iodine for double-contrast dual-energy CT of the bowel. Contrast Media Mol Imaging. 2016 epub ahead of print.
44. Brooks RA, Chiro GD. Beam hardening in X-ray reconstructive tomography. Phys Med Biol. 1976; 21:390. [PubMed: 778862]
45. Schindera ST, Tock I, Marin D, Nelson RC, Raupach R, Hagemeister M, Allmen Gv, Vock P, Szucs-Farkas Z. Effect of Beam Hardening on Arterial Enhancement in Thoracoabdominal CT Angiography with Increasing Patient Size: An in Vitro and in Vivo Study. Radiology. 2010; 256:528–535. [PubMed: 20656839]
46. Yu L, Leng S, McCollough CH. Dual-Energy CT–Based Monochromatic Imaging. Am J Roentgenol. 2012; 199:S9–S15. [PubMed: 23097173]
47. Bamberg F, Dierks A, Nikolaou K, Reiser MF, Becker CR, Johnson TR. Metal artifact reduction by dual energy computed tomography using monoenergetic extrapolation. Eur Radiol. 2011; 21:1424–1429. [PubMed: 21249370]
48. De Cecco, CN., Laghi, A., Schoepf, UJ., Meinel, FG. Dual Energy CT in Oncology. Springer; 2015.
49. Marin D, Boll DT, Mileto A, Nelson RC. State of the art: dual-energy CT of the abdomen. Radiology. 2014; 271:327–342. [PubMed: 24761954]
50. Yu L, Primak AN, Liu X, McCollough CH. Image quality optimization and evaluation of linearly mixed images in dual-source, dual-energy CT. Medical physics. 2009; 36:1019–1024. [PubMed: 19378762]
51. Johnson TR, Krauss B, Sedlmair M, Grasruck M, Bruder H, Morhard D, Fink C, Weckbach S, Lenhard M, Schmidt B, Flohr T, Reiser MF, Becker CR. Material differentiation by dual energy CT: initial experience. European radiology. 2007; 17:1510–1517. [PubMed: 17151859]
52. Liu X, Yu L, Primak AN, McCollough CH. Quantitative imaging of element composition and mass fraction using dual-energy CT: three-material decomposition. Med Phys. 2009; 36:1602–1609. [PubMed: 19544776]
53. Mendonça PR, Lamb P, Sahani DV. A flexible method for multi-material decomposition of dual-energy CT images, Medical Imaging. IEEE Transactions on. 2014; 33:99–116.
54. Fuchs TA, Stehli J, Dougoud S, Sah BR, Bull S, Clerc OF, Possner M, Buechel RR, Gaemperli O, Kaufmann PA. Coronary artery calcium quantification from contrast enhanced CT using gemstone spectral imaging and material decomposition. The international journal of cardiovascular imaging. 2014; 30:1399–1405. [PubMed: 24993390]

55. Mileto A, Mazziotti S, Gaeta M, Bottari A, Zimbaro F, Giardina C, Ascenti G. Pancreatic dual-source dual-energy CT: is it time to discard unenhanced imaging? Clin Radiol. 2012; 67:334–339. [PubMed: 22094183]
56. De Cecco CN, Buffa V, Fedeli S, Luzietti M, Vallone A, Ruopoli R, Miele V, Rengo M, Paolantonio P, Maurizi Enrici M, Laghi A, David V. Dual energy CT (DECT) of the liver: conventional versus virtual unenhanced images. Eur Radiol. 2010; 20:2870–2875. [PubMed: 20623126]
57. Ascenti G, Mileto A, Krauss B, Gaeta M, Blandino A, Scribano E, Settineri N, Mazziotti S. Distinguishing enhancing from nonenhancing renal masses with dual-source dual-energy CT: iodine quantification versus standard enhancement measurements. Eur Radiol. 2013; 23:2288–2295. [PubMed: 23479222]
58. Nicolaou S, Liang T, Murphy DT, Korzan JR, Ouellette H, Munk P. Dual-energy CT: a promising new technique for assessment of the musculoskeletal system. Am J Roentgenol. 2012; 199:S78–S86. [PubMed: 23097171]
59. Fischer MA, Reiner CS, Raptis D, Donati O, Goetti R, Clavien PA, Alkadhi H. Quantification of liver iron content with CT—added value of dual-energy. Eur Radiol. 2011; 21:1727–1732. [PubMed: 21472472]
60. Tran DN, Straka M, Roos JE, Napel S, Fleischmann D. Dual-energy CT discrimination of iodine and calcium: experimental results and implications for lower extremity CT angiography. Acad Radiol. 2009; 16:160–171. [PubMed: 19124101]
61. Fischer MA, Gnannt R, Raptis D, Reiner CS, Clavien PA, Schmidt B, Leschka S, Alkadhi H, Goetti R. Quantification of liver fat in the presence of iron and iodine: an ex-vivo dual-energy CT study. Invest Radiol. 2011; 46:351–358. [PubMed: 21263329]
62. Thomas C, Krauss B, Ketelsen D, Tsiflikas I, Reimann A, Werner M, Schilling D, Hennenlotter J, Claussen CD, Schlemmer HP. Differentiation of urinary calculi with dual energy CT: effect of spectral shaping by high energy tin filtration. Invest Radiol. 2010; 45:393–398. [PubMed: 20440214]
63. Lell M, May M, Brand M, Eller A, Buder T, Hofmann E, Uder M, Wuest W. Imaging the Parasinus Region with a Third-Generation Dual-Source CT and the Effect of Tin Filtration on Image Quality and Radiation Dose. American Journal of Neuroradiology. 2015
64. Schenzle JC, Sommer WH, Neumaier K, Michalski G, Lechel U, Nikolaou K, Becker CR, Reiser MF, Johnson TRC. Dual Energy CT of the Chest: How About the Dose? Invest Radiol. 2010; 45:347–353. [PubMed: 20404737]
65. Li M, Zhang GM, Zhao JS, Jiang ZW, Peng ZH, Jin ZT, Sun G. Diagnostic performance of dual-source CT coronary angiography with and without heart rate control: systematic review and meta-analysis. Clin Radiol. 2014; 69:163–171. [PubMed: 24268513]
66. Russo V, Garattoni M, Buia F, Attinà D, Lovato L, Zompatori M. 128-slice CT angiography of the aorta without ECG-gating: efficacy of faster gantry rotation time and iterative reconstruction in terms of image quality and radiation dose. Eur Radiol. 2016; 26:359–369. [PubMed: 26003792]
67. Aghayev A, Murphy DJ, Keraliya AR, Steigner ML. Recent developments in the use of computed tomography scanners in coronary artery imaging. Expert Rev Med Devices. 2016; 13:545–553. [PubMed: 27140944]
68. Siewerdsen JH, Jaffray DA. Cone-beam computed tomography with a flat-panel imager: magnitude and effects of x-ray scatter. Med Phys. 2001; 28:220–231. [PubMed: 11243347]
69. Kalender WA, Kyriakou Y. Flat-detector computed tomography (FD-CT). Eur Radiol. 2007; 17:2767–2779. [PubMed: 17587058]
70. Endo M, Mori S, Tsunoo T, Miyazaki H. Magnitude and effects of x-ray scatter in a 256-slice CT scanner. Med Phys. 2006; 33:3359–3368. [PubMed: 17022232]
71. Luhta, RP., Mattson, RA., Harwood, BE. Detector array with pre-focused anti-scatter grid. US. 8525119. 2013.
72. Melnyk, R., Boudry, J., Liu, X., Adamak, M. Anti-scatter grid evaluation for wide-cone CT. Proc. SPIE, Medical Imaging; San Diego. 2014; p. 90332P

73. Flohr, T., Schmidt, B. Technical Aspects of Dual Energy CT with Dual Source CT Systems. In: Carrascosa, PM.Cury, RC.García, MJ., Leipsic, JA., editors. Dual-Energy CT in Cardiovascular Imaging. Springer; 2015. p. 11-32.
74. Den Harder AM, Willemink MJ, De Ruiter QM, De Jong PA, Schilham AM, Krestin GP, Leiner T, Budde RP. Dose reduction with iterative reconstruction for coronary CT angiography: a systematic review and meta-analysis. Br J Radiol. 2016; 89:20150068. [PubMed: 26562096]
75. Benjaminov, O., Perlow, E., Romman, Z., Levinson, R., Bashara, B., Cohen, M., Zelikovsky, A. Novel Energy-Discriminating Photon Counting CT System (EDCT): First Clinical Evaluation—CT Angiography: Carotid Artery Stenosis. Radiological Society of North America 2008 Scientific Assembly and Annual Meeting; Chicago IL. 2008;
76. Romman, Z., Benjaminov, O., Levinson, R., Arenson, J., Ben-Basat, C., Cohen, M., Chabatov, G., Shimon, I. Virtual Noncontrast CT of the Abdomen Using a Dual Energy Photon-counting CT Scanner: Assessment of Performance. Radiological Society of North America 2009 Scientific Assembly and Annual Meeting; Chicago IL. 2009;
77. Pourmorteza A, Symons R, Sandfort V, Mallek M, Fuld MK, Henderson G, Jones EC, Malayeri AA, Folio LR, Bluemke DA. Abdominal Imaging with Contrast-enhanced Photon-counting CT: First Human Experience. Radiology. 2016; 279:239–245. [PubMed: 26840654]
78. Yu Z, Leng S, Jorgensen SM, Li Z, Gutjahr R, Chen B, Halaweish AF, Kappler S, Yu L, Ritman EL, McCollough CH. Evaluation of conventional imaging performance in a research whole-body CT system with a photon-counting detector array. Phys Med Biol. 2016; 61:1572–1595. [PubMed: 26835839]
79. Donath T, Pfeiffer F, Bunk O, Grunzweig C, Hempel E, Popescu S, Vock P, David C. Toward clinical X-ray phase-contrast CT: demonstration of enhanced soft-tissue contrast in human specimen. Investigative radiology. 2010; 45:445–452. [PubMed: 20498610]
80. Bech M, Jensen TH, Bunk O, Donath T, David C, Weitkamp T, Le Duc G, Bravin A, Cloetens P, Pfeiffer F. Advanced contrast modalities for X-ray radiology: Phase-contrast and dark-field imaging using a grating interferometer. Zeitschrift fur medizinische Physik. 2010; 20:7–16. [PubMed: 20211422]
81. Momose A, Yashiro W, Kido K, Kiyohara J, Makifuchi C, Ito T, Nagatsuka S, Honda C, Noda D, Hattori T, Endo T, Nagashima M, Tanaka J. X-ray phase imaging: from synchrotron to hospital, Philosophical transactions. Series A, Mathematical, physical and engineering sciences. 2014; 372:20130023.
82. McDonald RJ, McDonald JS, Newhouse JH, Davenport MS. Controversies in Contrast Material–induced Acute Kidney Injury: Closing in on the Truth? Radiology. 2015; 277:627–632. [PubMed: 26599922]
83. Subramaniam RM, Suarez-Cuervo C, Wilson RF, Turban S, Zhang A, Sherrod C, Aboagye J, Eng J, Choi MJ, Hutfless S, Bass EB. Effectiveness of Prevention Strategies for Contrast-Induced NephropathyA Systematic Review and Meta-analysisEffectiveness of Prevention Strategies for CIN. Annals of Internal Medicine. 2016; 164:406–416. [PubMed: 26830221]
84. Dong J, Wang X, Jiang X, Gao L, Li F, Qiu J, Xu Y, Wang H. Low-Contrast Agent Dose Dual-Energy CT Monochromatic Imaging in Pulmonary Angiography Versus Routine CT. Journal of computer assisted tomography. 2013; 37:618–625. [PubMed: 23863541]
85. Lu GM, Wu SY, Yeh BM, Zhang LJ. Dual-energy computed tomography in pulmonary embolism. The British Journal of Radiology. 2010; 83:707–718. [PubMed: 20551257]
86. Shuman WP, Chan KT, Busey JM, Mitsumori LM, Koprowicz KM. Dual-energy CT Aortography with 50% Reduced Iodine Dose Versus Single-energy CT Aortography with Standard Iodine Dose. Academic radiology. 2016; 23:611–618. [PubMed: 26897602]
87. Frank I, Blute ML, Cheville JC, Lohse CM, Weaver AL, Zincke H. Solid Renal Tumors: An Analysis of Pathological Features Related to Tumor Size. The Journal of Urology. 2003; 170:2217–2220. [PubMed: 14634382]
88. Qu M, Ehman E, Fletcher JG, Huprich JE, Hara AK, Silva AC, Farrugia G, Limburg P, McCollough CH. Toward biphasic computed tomography (CT) enteric contrast: material classification of luminal bismuth and mural iodine in a small-bowel phantom using dual-energy CT. Journal of computer assisted tomography. 2012; 36:554–559. [PubMed: 22992606]

89. Clark DP, Ghaghada K, Moding EJ, Kirsch DG, Badea CT. In vivo characterization of tumor vasculature using iodine and gold nanoparticles and dual energy micro-CT. Physics in Medicine and Biology. 2013; 58:1683–1704. [PubMed: 23422321]

90. Anderson NG, Butler AP, Scott NJA, Cook NJ, Butzer JS, Schleich N, Firsching M, Grasset R, de Ruiter N, Campbell M, Butler PH. Spectroscopic (multi-energy) CT distinguishes iodine and barium contrast material in MICE. European radiology. 2010; 20:2126–2134. [PubMed: 20309554]

91. Raatschen HJ, Fu Y, Brasch RC, Pietsch H, Shames DM, Yeh BM. In vivo monitoring of angiogenesis inhibitory treatment effects by dynamic contrast-enhanced computed tomography in a xenograft tumor model. Investigative radiology. 2009; 44:265–270. [PubMed: 19346961]

92. Bhavane R, Badea C, Ghaghada KB, Clark D, Vela D, Moturu A, Annapragada A, Johnson GA, Willerson JT, Annapragada A. Dual-energy computed tomography imaging of atherosclerotic plaques in a mouse model using a liposomal-iodine nanoparticle contrast agent. Circulation. Cardiovascular imaging. 2013; 6:285–294. [PubMed: 23349231]

93. Ashton JR, Befera N, Clark D, Qi Y, Mao L, Rockman HA, Johnson GA, Badea CT. Anatomical and functional imaging of myocardial infarction in mice using micro-CT and eXIA 160 contrast agent. Contrast media & molecular imaging. 2014; 9:161–168. [PubMed: 24523061]

94. McGinnity TL, Dominguez O, Curtis TE, Nallathamby PD, Hoffman AJ, Roeder RK. Hafnia (HfO2) nanoparticles as an X-ray contrast agent and mid-infrared biosensor. Nanoscale. 2016

95. Li X, Anton N, Zuber G, Vandamme T. Contrast agents for preclinical targeted X-ray imaging. Advanced Drug Delivery Reviews. 2014; 76:116–133. [PubMed: 25086373]

96. Wang Y, Jiang C, He W, Ai K, Ren X, Liu L, Zhang M, Lu L. Targeted Imaging of Damaged Bone in Vivo with Gemstone Spectral Computed Tomography. ACS Nano. 2016; 10:4164–4172. [PubMed: 27043072]

97. Wang ZJ, Yeh BM, Roberts JP, Breiman RS, Qayyum A, Coakley FV. Living Donor Candidates for Right Hepatic Lobe Transplantation: Evaluation at CT Cholangiography—Initial Experience. Radiology. 2005; 235:899–904. [PubMed: 15833987]

98. Idée J-M, Guiu B. Use of Lipiodol as a drug-delivery system for transcatheter arterial chemoembolization of hepatocellular carcinoma: A review. Critical Reviews in Oncology/ Hematology. 2013; 88:530–549. [PubMed: 23921081]

99. Behan M, O'Connell D, Mattrey RF, Carney DN. Perfluorooctylbromide as a contrast agent for CT and sonography: preliminary clinical results. American Journal of Roentgenology. 1993; 160:399–405. [PubMed: 8424361]

100. Jin E, Lu Z-R. Biodegradable iodinated polydisulfides as contrast agents for CT angiography. Biomaterials. 2014; 35:5822–5829. [PubMed: 24768156]

101. Raatschen H-J, Fu Y, Brasch RC, Pietsch H, Shames DM, Yeh BM. In Vivo Monitoring of Angiogenesis Inhibitory Treatment Effects by Dynamic Contrast-Enhanced Computed Tomography in a Xenograft Tumor Model. Investigative radiology. 2009; 44:265–270. [PubMed: 19346961]

102. Yu S-B, Watson AD. Metal-Based X-ray Contrast Media. Chemical Reviews. 1999; 99:2353–2378. [PubMed: 11749484]

103. Emsley, J. Nature's Building Blocks: An A-Z Guide to the Elements. Oxford University Press; 2001.

104. U.S. Geological Survey. Mineral Commodity summaries. 2015.

105. Kaye, Laby, editors. 4.2.1 X-ray absorption edges, characteristic X-ray lines and fluorescent yields. 2005. Tables of Physical & Chemical Constants (16th edition 1995).

106. FitzGerald PF, Colborn RE, Edic PM, Lambert JW, Torres AS, Peter J, Bonitatibus J, Yeh BM. CT Image Contrast of High-Z Elements: Phantom Imaging Studies and Clinical Implications. Radiology. 2016; 278:723–733. [PubMed: 26356064]

107. Lee N, Choi SH, Hyeon T. Nano-sized CT contrast agents. Adv Mater. 2013; 25:2641–2660. [PubMed: 23553799]

108. Cormode DP, Naha PC, Fayad ZA. Nanoparticle contrast agents for computed tomography: A focus on micelles. Contrast Media and Molecular Imaging. 2014; 9:37–52. [PubMed: 24470293]

109. Hahn MA, Singh AK, Sharma P, Brown SC, Moudgil BM. Nanoparticles as contrast agents for in-vivo bioimaging: Current status and future perspectives. Analytical and Bioanalytical Chemistry. 2011; 399:3–27. [PubMed: 20924568]
110. Liu Y, Ai K, Lu L. Nanoparticulate X-ray computed tomography contrast agents: From design validation to in vivo applications. Accounts of Chemical Research. 2012; 45:1817–1827. [PubMed: 22950890]
111. Lusic H, Grinstaff MW. X-Ray Computed Tomography Contrast Agents. Chemical reviews. 2013; 113:1641–1666. [PubMed: 23210836]
112. De La Vega JC, Häfeli UO. Utilization of nanoparticles as X-ray contrast agents for diagnostic imaging applications. Contrast media & molecular imaging. 2015; 10:81–95. [PubMed: 25044541]
113. Kang H, Mintri S, Menon AV, Lee HY, Choi HS, Kim J. Pharmacokinetics, pharmacodynamics and toxicology of theranostic nanoparticles. Nanoscale. 2015; 7:18848–18862. [PubMed: 26528835]
114. Mortelé KJ, Oliva MR, Ondategui S, Ros PR, Silverman SG. Universal use of nonionic iodinated contrast medium for CT: Evaluation of safety in a large urban teaching hospital. American Journal of Roentgenology. 2005; 184:31–34. [PubMed: 15615946]
115. Roh S, Laroia A. Practicing Safe Use of Nonionic Low-osmolarity Iodinated Contrast. Applied Radiology. 2015; 44:16–19.
116. Seeliger E, Sendeski M, Rihal CS, Persson PB. Contrast-induced kidney injury: mechanisms, risk factors, and prevention. European Heart Journal. 2012; 33:2007–2015. [PubMed: 22267241]
117. Meurer K, Kelsch B, Hogstrom B. The pharmacokinetic profile, tolerability and safety of the iodinated, non-ionic, dimeric contrast medium Iosimenol 340 injection in healthy human subjects. Acta Radiologica. 2015; 56:581–586. [PubMed: 24895062]
118. Wistrand LG, Rogstad A, Hagelin G, Roed L, Oulie I, Gram A, Evans P, Rasmussen H, Grant D, Iveson P, Newton B, Thaning M. GE-145, a new low-osmolar dimeric radiographic contrast medium. Acta Radiologica. 2010; 51:1014–1020. [PubMed: 20849319]
119. Chai CM, Rasmussen H, Eriksen M, Hvoslef AM, Evans P, Newton BB, Videm S. Predicting cardiotoxicity propensity of the novel iodinated contrast medium GE-145: Ventricular fibrillation during left coronary arteriography in pigs. Acta Radiologica. 2010; 51:1007–1013. [PubMed: 20799918]
120. Eng J, Wilson RF, Subramaniam RM, Zhang A, Suarez-Cuervo C, Turban S, Choi MJ, Sherrod C, Hutfless S, Iyoha EE, Bass EB. Comparative Effect of Contrast Media Type on the Incidence of Contrast-Induced NephropathyA Systematic Review and Meta-analysisComparative Effect of Contrast Media Type. Annals of Internal Medicine. 2016; 164:417–424. [PubMed: 26830055]
121. FitzGerald PF, Butts MD, Roberts JC, Colborn RE, Torres AS, Lee BD, Yeh BM, Bonitatibus PJJ. A Proposed Computed Tomography Contrast Agent Using Carboxybetaine Zwitterionic Tantalum Oxide Nanoparticles: Imaging, Biological, and Physicochemical Performance, Investigative radiology. Publish Ahead of Print. 2016
122. Hallouard F, Anton N, Choquet P, Constantinesco A, Vandamme T. Iodinated blood pool contrast media for preclinical X-ray imaging applications - A review. Biomaterials. 2010; 31:6249–6268. [PubMed: 20510444]
123. deKrafft KE, Xie Z, Cao G, Tran S, Ma L, Zhou OZ, Lin W. Iodinated Nanoscale Coordination Polymers as Potential Contrast Agents for Computed Tomography. Angewandte Chemie. 2009; 121:10085–10088.
124. Fu Y, Nitecki DE, Maltby D, Simon GH, Berejnoi K, Raatschen H-J, Yeh BM, Shames DM, Brasch RC. Dendritic Iodinated Contrast Agents with PEG-Cores for CT Imaging: Synthesis and Preliminary Characterization. Bioconjugate Chemistry. 2006; 17:1043–1056. [PubMed: 16848414]
125. de Vries A, Custers E, Lub J, van den Bosch S, Nicolay K, Grüll H. Block-copolymer-stabilized iodinated emulsions for use as CT contrast agents. Biomaterials. 2010; 31:6537–6544. [PubMed: 20541800]
126. Attia MF, Anton N, Chiper M, Akasov R, Anton H, Messaddeq N, Fournel S, Klymchenko AS, Mély Y, Vandamme TF. Biodistribution of X-Ray Iodinated Contrast Agent in Nano-Emulsions

Is Controlled by the Chemical Nature of the Oily Core. ACS Nano. 2014; 8:10537–10550. [PubMed: 25284066]

127. Torchilin VP, Frank-Kamenetsky MD, Wolf GL. CT visualization of blood pool in rats by using long-circulating, iodine-containing micelles. Academic radiology. 1999; 6:61–65. [PubMed: 9891154]
128. Pan D, Williams TA, Senpan A, Allen JS, Scott MJ, Gaffney PJ, Wickline SA, Lanza GM. Detecting Vascular Biosignatures with a Colloidal, Radio-Opaque Polymeric Nanoparticle. Journal of the American Chemical Society. 2009; 131:15522–15527. [PubMed: 19795893]
129. Yin Q, Yap FY, Yin L, Ma L, Zhou Q, Dobrucki LW, Fan TM, Gaba RC, Cheng J. Poly(iohexol) Nanoparticles As Contrast Agents for in Vivo X-ray Computed Tomography Imaging. Journal of the American Chemical Society. 2013; 135:13620–13623. [PubMed: 23987119]
130. Hyafil F, Cornily JC, Feig JE, Gordon R, Vucic E, Amirbekian V, Fisher EA, Fuster V, Feldman LJ, Fayad ZA. Noninvasive detection of macrophages using a nanoparticulate contrast agent for computed tomography. Nature Medicine. 2007; 13:636–641.
131. Starosolski Z, Villamizar CA, Rendon D, Paldino MJ, Milewicz DM, Ghaghada KB, Annapragada AV. Ultra High-Resolution In vivo Computed Tomography Imaging of Mouse Cerebrovasculature Using a Long Circulating Blood Pool Contrast Agent. Scientific Reports. 2015; 5:10178. [PubMed: 25985192]
132. Clark, DP., Touch, M., Barber, W., Badea, CT. SPIE Medical Imaging. Orlando, FL: 2015. Simultaneous imaging of multiple contrast agents using full-spectrum micro-CT; p. 941222–941222-941212.
133. Lambert, JW., Edic, PM., Fitzgerald, P., Torres, AS., Yeh, BM. Complementary contrast media for metal artifact reduction in dual-energy CT. SPIE Proceedings; 2015; p. 941203–941203-941212.
134. Meagher M, Leone B, Turnbull T, Ross R, Zhang Z, Roeder R. Dextran-encapsulated barium sulfate nanoparticles prepared for aqueous dispersion as an X-ray contrast agent. Journal of Nanoparticle Research. 2013; 15:1–10.
135. Kim SJ, Xu W, Ahmad MW, Baeck JS, Chang Y, Bae JE, Chae KS, Kim TJ, Park JA, Lee GH. Synthesis of nanoparticle CT contrast agents:in vitro and in vivo studies. Science and Technology of Advanced Materials. 2015; 16:055003. [PubMed: 27877838]
136. Liu Z, Ju E, Liu J, Du Y, Li Z, Yuan Q, Ren J, Qu X. Direct visualization of gastrointestinal tract with lanthanide-doped BaYbF5 upconversion nanoprobes. Biomaterials. 2013; 34:7444–7452. [PubMed: 23849344]
137. Liu Y, Ai K, Liu J, Yuan Q, He Y, Lu L. Hybrid BaYbF5nanoparticles: Novel binary contrast agent for high-resolution in vivo X-ray computed tomography angiography. Advanced Healthcare Materials. 2012; 1:461–466. [PubMed: 23184777]
138. Wang J, Ni D, Bu W, Zhou Q, Fan W, Wu Y, Liu Y, Yin L, Cui Z, Zhang X, Zhang H, Yao Z. $BaHoF_5$ nanoprobes as high-performance contrast agents for multi-modal CT imaging of ischemic stroke. Biomaterials. 2015; 71:110–118. [PubMed: 26321059]
139. Sase S, Takahashi H, Shigefuku R, Ikeda H, Kobayashi M, Matsumoto N, Suzuki M. Measurement of blood flow and xenon solubility coefficient in the human liver by xenon-enhanced computed tomography. Medical physics. 2012; 39:7553–7559. [PubMed: 23231303]
140. Cao W, Cheng X, Li H, Wang L, Zhang X, Dong Q. Evaluation of cerebrovasculREserve using xenon-enhanced CT scanning in patients with symptomatic middle cerebral artery stenosis. Journal of Clinical Neuroscience. 2014; 21:293–297. [PubMed: 24238634]
141. Kim WW, Lee CH, Goo JM, Park SJ, Kim JH, Park E-A, Cho S-H. Xenon-Enhanced Dual-Energy CT of Patients With Asthma: Dynamic Ventilation Changes After Methacholine and Salbutamol Inhalation. American Journal of Roentgenology. 2012; 199:975–981. [PubMed: 23096168]
142. Kong X, Sheng HX, Lu GM, Meinel FG, Dyer KT, Schoepf UJ, Zhang LJ. Xenon-Enhanced Dual-Energy CT Lung Ventilation Imaging: Techniques and Clinical Applications. American Journal of Roentgenology. 2014; 202:309–317. [PubMed: 24450670]
143. Wang Q, Yu Y, Pan K, Liu J. Liquid metal angiography for mega contrast X-ray visualization of vascular network in reconstructing in-vitro organ anatomy. IEEE Trans Biomed Eng. 2014; 61:2161–2166. [PubMed: 24759980]

144. Keogan DM, Griffith DM. Current and potential applications of bismuth-based drugs. Molecules. 2014; 19:15258–15297. [PubMed: 25251194]

145. Rabin O, Manuel Perez J, Grimm J, Wojtkiewicz G, Weissleder R. An X-ray computed tomography imaging agent based on long-circulating bismuth sulphide nanoparticles. Nature Materials. 2006; 5:118–122. [PubMed: 16444262]

146. Chen J, Yang XQ, Meng YZ, Huang HH, Qin MY, Yan DM, Zhao YD, Ma ZY. In vitro and in vivo CT imaging using bismuth sulfide modified with a highly biocompatible Pluronic F127. Nanotechnology. 2014; 25

147. Fang Y, Peng C, Guo R, Zheng L, Qin J, Zhou B, Shen M, Lu X, Zhang G, Shi X. Dendrimer-stabilized bismuth sulfide nanoparticles: Synthesis, characterization, and potential computed tomography imaging applications. Analyst. 2013; 138:3172–3180. [PubMed: 23616984]

148. Kinsella JM, Jimenez RE, Karmali PP, Rush AM, Kotamraju VR, Gianneschi NC, Ruoslahti E, Stupack D, Sailor MJ. X-ray computed tomography imaging of breast cancer by using targeted peptide-labeled bismuth sulfide nanoparticles. Angew Chem Int Ed Engl. 2011; 50:12308–12311. [PubMed: 22028313]

149. Aviv H, Bartling S, Grinberg I, Margel S. Synthesis and characterization of Bi2O3/HSA core-shell nanoparticles for X-ray imaging applications. Journal of Biomedical Materials Research - Part B Applied Biomaterials. 2013; 101 B:131–138.

150. Rivera EJ, Tran LA, Hernandez-Rivera M, Yoon D, Mikos AG, Rusakova IA, Cheong BY, Cabreira-Hansen MdG, Willerson JT, Perin EC, Wilson LJ. Bismuth@US-tubes as a potential contrast agent for X-ray imaging applications. Journal of Materials Chemistry B. 2013; 1:4792–4800.

151. Brown AL, Naha PC, Benavides-Montes V, Litt HI, Goforth AM, Cormode DP. Synthesis, X-ray Opacity, and Biological Compatibility of Ultra-High Payload Elemental Bismuth Nanoparticle X-ray Contrast Agents. Chemistry of Materials. 2014; 26:2266–2274. [PubMed: 24803727]

152. Pan D, Roessl E, Schlomka J-P, Caruthers SD, Senpan A, Scott MJ, Allen JS, Zhang H, Hu G, Gaffney PJ, Choi ET, Rasche V, Wickline SA, Proksa R, Lanza GM. Computed Tomography in Color: NanoK-Enhanced Spectral CT Molecular Imaging. Angewandte Chemie International Edition. 2010; 49:9635–9639. [PubMed: 21077082]

153. Branca M, Pelletier F, Cottin B, Ciuculescu D, Lin CC, Serra R, Mattei JG, Casanove MJ, Tan R, Respaud M, Amiens C. Design of FeBi nanoparticles for imaging applications. Faraday Discussions. 2014; 175:97–111. [PubMed: 25271897]

154. Naha PC, Al Zaki A, Hecht E, Chorny M, Chhour P, Blankemeyer E, Yates DM, Witschey WRT, Litt HI, Tsourkas A, Cormode DP. Dextran coated bismuth-iron oxide nanohybrid contrast agents for computed tomography and magnetic resonance imaging. Journal of Materials Chemistry B. 2014; 2:8239–8248.

155. Andrés-Vergés M, del Puerto Morales M, Veintemillas-Verdaguer S, Palomares FJ, Serna CJ. Core/Shell Magnetite/Bismuth Oxide Nanocrystals with Tunable Size, Colloidal, and Magnetic Properties. Chemistry of Materials. 2012; 24:319–324.

156. Zheng X, Shi J, Bu Y, Tian G, Zhang X, Yin W, Gao B, Yang Z, Hu Z, Liu X, Yan L, Gu Z, Zhao Y. Silica-coated bismuth sulfide nanorods as multimodal contrast agents for a non-invasive visualization of the gastrointestinal tract. Nanoscale. 2015; 7:12581–12591. [PubMed: 26145146]

157. Ba Z, Zhang Y, Wei J, Han J, Wang Z, Shao G. Large-scale synthesis of PEGylated lutetium hydroxycarbonates as nanoparticulate contrast agents for X-ray CT imaging. New Journal of Chemistry. 2015; 39:589–594.

158. Yi Z, Lu W, Xu Y, Yang J, Deng L, Qian C, Zeng T, Wang H, Rao L, Liu H, Zeng S. PEGylated NaLuF4: Yb/Er upconversion nanophosphors for in vivo synergistic fluorescence/X-ray bioimaging and long-lasting, real-time tracking. Biomaterials. 2014; 35:9689–9697. [PubMed: 25176069]

159. Zhuravleva EY. Tantalum X-ray Contrast Media(Solid-State Chemistry for MedicineSeries), by M. G. Zuev and L. P. Larionov, Yekaterinburg: Ural. Otd., Ross. Akad. Nauk, 2002. Inorganic Materials. 2004; 40:671–672.

160. Yang WM, Liu YW, Zhang Q, Leng YX, Zhou HF, Yang P, Chen JY, Huang N. Biomedical response of tantalum oxide films deposited by DC reactive unbalanced magnetron sputtering. Surface and Coatings Technology. 2007; 201:8062–8065.

161. Mullan BF, Madsen MT, Messerle L, Kolesnichenko V, Kruger J. X-ray attenuation coefficients of high-atomic-number, hexanuclear transition metal cluster compounds: A new paradigm for radiographic contrast agents. Academic radiology. 2000; 7:254–259. [PubMed: 10766098]

162. Gamsu G, Platzker A, Gregory G, Graf P, Nadel JA. Powdered tantalum as a contrast agent for tracheobronchography in the pediatric patient. Radiology. 1973; 107:151–157. [PubMed: 4689423]

163. Nadel JA, Wolfe WG, Graf PD. Powdered Tantalum as a Medium for Bronchography in Canine and Human Lungs. Investigative radiology. 1968; 3:229–237. [PubMed: 5678890]

164. Margulis AR, Stoughton JA, Stein LA. Non-contractile movement of tantalum powder in the canine rectum. Am J Roentgenol Radium Ther Nucl Med. 1975; 125:244–250.

165. Smith JC, Stitik FP, Swift DL. Airway Visualization by Tantalum Inhalation Bronchography. American Review of Respiratory Disease. 1976; 113:515–529. [PubMed: 1267258]

166. Bonitatibus PJ Jr, Torres AS, Goddard GD, FitzGerald PF, Kulkarni AM. Synthesis, characterization, and computed tomography imaging of a tantalum oxide nanoparticle imaging agent. Chemical Communications. 2010; 46:8956. [PubMed: 20976321]

167. Bonitatibus PJ, Torres AS, Kandapallil B, Lee BD, Goddard GD, Colborn RE, Marino ME. Preclinical Assessment of a Zwitterionic Tantalum Oxide Nanoparticle X-ray Contrast Agent. ACS Nano. 2012; 6:6650–6658. [PubMed: 22768795]

168. Torres AS, Bonitatibus PJ Jr, Colborn RE, Goddard GD, FitzGerald PF, Lee BD, Marino ME. Biological performance of a size-fractionated core-shell tantalum oxide nanoparticle x-ray contrast agent. Investigative radiology. 2012; 47:578–587. [PubMed: 22836312]

169. Oh MH, Lee N, Kim H, Park SP, Piao Y, Lee J, Jun SW, Moon WK, Choi SH, Hyeon T. Large-scale synthesis of bioinert tantalum oxide nanoparticles for X-ray computed tomography imaging and bimodal image-guided sentinel lymph node mapping. Journal of the American Chemical Society. 2011; 133:5508–5515. [PubMed: 21428437]

170. Wang, X., Wang, C., Anderson, S., Zhang, X. Fabrication of hydrogel particles with tantalum oxide nanoparticle payloads as computed tomography contrast agents. 2013 Transducers and Eurosensors XXVII: The 17th International Conference on Solid-State Sensors, Actuators and Microsystems, TRANSDUCERS and EUROSENSORS 2013; 2013; p. 426-429.

171. Bonitatebus, PJ., Axelsson, OHE., Kulkarni, AM., Bales, BC., Walter, DJ., Torres, AS., Treynor, C. Nanoparticle-based imaging agents for X-ray/computed tomography. US. 20070098641. 2007.

172. Roberts, J., Bonitatibus, P., Butts, M., Colborn, RE., Edic, P., Fitzgerald, PF., Lambert, J., Marino, M., Torres, A., Yeh, B. Physiochemical, biological, and imaging performance of zwitterionic-coated TaO nanoparticles as CT contrast agents. World Molecular Imaging Congress; Honolulu, HI. 2015;

173. Sovak M, Terry R, Abramjuk C, Faberova V, Fiserova M, Laznicek M, Leuschner J, Malinak J, Zahradnik P, Masner O, Seligson A. Iosimenol, a low-viscosity nonionic dimer: preclinical physicochemistry, pharmacology, and pharmacokinetics. Investigative radiology. 2004; 39:171–181. [PubMed: 15076009]

174. Jin Y, Li Y, Ma X, Zha Z, Shi L, Tian J, Dai Z. Encapsulating tantalum oxide into polypyrrole nanoparticles for X-ray CT/photoacoustic bimodal imaging-guided photothermal ablation of cancer. Biomaterials. 2014; 35:5795–5804. [PubMed: 24746966]

175. Hay DNT, Swenson DC, Messerle L, Gallium, Dichloride Gallium. New Solid-State Reductants in Preparative Transition Metal Chemistry. New, Lower Temperature Syntheses and Convenient Isolation of Hexatantalum Tetradecachloride Octahydrate, Ta6(μ-Cl)12Cl2(OH2)4.4H2O, and Synthesis and Solid-State Structure of a Tetraalkylammonium Derivative, [N(CH2Ph)Bu3]4[Ta6(μ-Cl)12Cl6], of the Reduced [Ta6(μ-Cl)12]2+ Cluster Core1. Inorganic Chemistry. 2002; 41:4700–4707. [PubMed: 12206693]

176. Jakhmola A, Anton N, Anton H, Messaddeq N, Hallouard F, Klymchenko A, Mely Y, Vandamme TF. Poly-ε-caprolactone tungsten oxide nanoparticles as a contrast agent for X-ray computed tomography. Biomaterials. 2014; 35:2981–2986. [PubMed: 24393266]

177. Liu J, Han J, Kang Z, Golamaully R, Xu N, Li H, Han X. In vivo near-infrared photothermal therapy and computed tomography imaging of cancer cells using novel tungsten-based theranostic probe. Nanoscale. 2014; 6:5770–5776. [PubMed: 24736832]

178. Zhang Y, Li B, Cao Y, Qin J, Peng Z, Xiao Z, Huang X, Zou R, Hu J. Na0.3WO3 nanorods: a multifunctional agent for in vivo dual-model imaging and photothermal therapy of cancer cells. Dalton Transactions. 2015; 44:2771–2779. [PubMed: 25468402]

179. Dong K, Liu Z, Liu J, Huang S, Li Z, Yuan Q, Ren J, Qu X. Biocompatible and high-performance amino acids-capped MnWO4 nanocasting as a novel non-lanthanide contrast agent for X-ray computed tomography and T(1)-weighted magnetic resonance imaging. Nanoscale. 2014; 6:2211–2217. [PubMed: 24382605]

180. Giljohann DA, Seferos DS, Daniel WL, Massich MD, Patel PC, Mirkin CA. Gold Nanoparticles for Biology and Medicine. Angewandte Chemie (International ed in English). 2010; 49:3280–3294. [PubMed: 20401880]

181. Hainfeld JF, Slatkin DN, Focella TM, Smilowitz HM. Gold nanoparticles: A new X-ray contrast agent. British Journal of Radiology. 2006; 79:248–253. [PubMed: 16498039]

182. Cole LE, Ross RD, Tilley JMR, Vargo-Gogola T, Roeder RK. Gold nanoparticles as contrast agents in x-ray imaging and computed tomography. Nanomedicine. 2015; 10:321–341. [PubMed: 25600973]

183. Hainfeld, JF., Slatkin, DN. Media and methods for enhanced medical imaging. US: 2004.

184. Shi X, Wang S, Meshinchi S, Van Antwerp ME, Bi X, Lee I, Baker JR Jr. Dendrimer-entrapped gold nanoparticles as a platform for cancer-cell targeting and imaging. Small. 2007; 3:1245–1252. [PubMed: 17523182]

185. Li D, Wen S, Shi X. Dendrimer-entrapped metal colloids as imaging agents. Wiley Interdisciplinary Reviews: Nanomedicine and Nanobiotechnology. 2015; 7:678–690. [PubMed: 25641958]

186. Sutriyo, Mutalib A, Ristaniah, Anwar E, Radji M, Pujiyanto A, Purnamasari P, Joshita D, Adang HG. Synthesis of Gold Nanoparticles with Polyamidoamine (Pamam) Generation 4 Dendrimer as Stabilizing Agent for CT Scan Contrast Agent. Macromolecular Symposia. 2015; 353:96–101.

187. Zhu J, Fu F, Xiong Z, Shen M, Shi X. Dendrimer-entrapped gold nanoparticles modified with RGD peptide and alpha-tocopheryl succinate enable targeted theranostics of cancer cells. Colloids and Surfaces B: Biointerfaces. 2015; 133:36–42. [PubMed: 26070049]

188. Cao Y, He Y, Liu H, Luo Y, Shen M, Xia J, Shi X. Targeted CT imaging of human hepatocellular carcinoma using low-generation dendrimer-entrapped gold nanoparticles modified with lactobionic acid. Journal of Materials Chemistry B. 2014; 3:286–295.

189. Song JT, Yang XQ, Zhang XS, Yan DM, Wang ZY, Zhao YD. Facile Synthesis of Gold Nanospheres Modified by Positively Charged Mesoporous Silica, Loaded with Near-Infrared Fluorescent Dye, for in Vivo X-ray Computed Tomography and Fluorescence Dual Mode Imaging. ACS Applied Materials and Interfaces. 2015; 7:17287–17297. [PubMed: 26189815]

190. Lai SF, Ko BH, Chien CC, Chang CJ, Yang SM, Chen HH, Petibois C, Hueng DY, Ka SM, Chen A, Margaritondo G, Hwu Y. Gold nanoparticles as multimodality imaging agents for brain gliomas. Journal of Nanobiotechnology. 2015; 13

191. Tian C, Zhu L, Lin F, Boyes SG. Poly(acrylic acid) Bridged Gadolinium Metal-Organic Framework-Gold Nanoparticle Composites as Contrast Agents for Computed Tomography and Magnetic Resonance Bimodal Imaging. ACS Applied Materials and Interfaces. 2015; 7:17765–17775. [PubMed: 26147906]

192. Karunamuni R, Tsourkas A, Maidment ADA. Exploring silver as a contrast agent for contrast-enhanced dual-energy X-ray breast imaging. British Journal of Radiology. 2014; 87:20140081. [PubMed: 24998157]

193. Liu H, Wang H, Guo R, Cao X, Zhao J, Luo Y, Shen M, Zhang G, Shi X. Size-controlled synthesis of dendrimer-stabilized silver nanoparticles for X-ray computed tomography imaging applications. Polymer Chemistry. 2010; 1:1677–1683.

194. Zou J, Hannula M, Misra S, Feng H, Labrador RH, Aula AS, Hyttinen J, Pyykko I. Micro CT visualization of silver nanoparticles in the middle and inner ear of rat and transportation pathway after transtympanic injection. J Nanobiotechnology. 2015; 13:5. [PubMed: 25622551]

195. Dong H, Du S-R, Zheng X-Y, Lyu G-M, Sun L-D, Li L-D, Zhang P-Z, Zhang C, Yan C-H. Lanthanide Nanoparticles: From Design toward Bioimaging and Therapy. Chemical Reviews. 2015; 115:10725–10815. [PubMed: 26151155]
196. Caravan P, Ellison JJ, McMurry TJ, Lauffer RB. Gadolinium(III) Chelates as MRI Contrast Agents: Structure, Dynamics, and Applications. Chemical Reviews. 1999; 99:2293–2352. [PubMed: 11749483]
197. Gierada DS, Bae KT. Gadolinium as a CT Contrast Agent: Assessment in a Porcine Model. Radiology. 1999; 210:829–834. [PubMed: 10207488]
198. Ahmad MW, Xu W, Kim SJ, Baeck JS, Chang Y, Bae JE, Chae KS, Park JA, Kim TJ, Lee GH. Potential dual imaging nanoparticle: Gd2O3 nanoparticle. Scientific Reports. 2015; 5
199. Kuo T, Lai W, Li C, Wun Y, Chang H, Chen J, Yang P, Chen C. AS1411 aptamer-conjugated Gd2O3:Eu nanoparticles for target-specific computed tomography/magnetic resonance/ fluorescence molecular imaging. Nano Research. 2014; 7:658–669.
200. Wu M, Li L, Yu X, Zhang D, Sun T, Li X, Sun L, Lui S, Huang X, Bi F, Wang H, Zhu H, Gong Q. Multifunctional layered gadolinium hydroxide nanoplates for ultrahigh field magnetic resonance imaging computed tomography and fluorescence bioimaging. Journal of biomedical nanotechnology. 2014; 10:3620–3630. [PubMed: 26000375]
201. Du Y, Xing M, Li Z, Guo W. PEGylated Gd(OH)3 nanorods as metabolizable contrast agents for computed tomography imaging. New Journal of Chemistry. 2015; 39:8999–9005.
202. Zeng S, Tsang MK, Chan CF, Wong KL, Hao J. PEG modified BaGdF5: Yb/Er nanoprobes for multi-modal upconversion fluorescent, in vivo X-ray computed tomography and biomagnetic imaging. Biomaterials. 2012; 33:9232–9238. [PubMed: 23036962]
203. Pietsch H, Jost G, Frenzel T, Raschke M, Walter J, Schirmer H, Hütter J, Sieber MA. Efficacy and safety of lanthanoids as X-ray contrast agents. European journal of radiology. 2011; 80:349–356. [PubMed: 20006455]
204. Reeder SB, Gulani V. Gadolinium Deposition in the Brain: Do We Know Enough to Change Practice? Radiology. 2016; 279:323–326.
205. Stojanov D, Aracki-Trenkic A, Benedeto-Stojanov D. Gadolinium deposition within the dentate nucleus and globus pallidus after repeated administrations of gadolinium-based contrast agents-current status. Neuroradiology. 2016; 58:433–441. [PubMed: 26873830]
206. Pan D, Schirra CO, Senpan A, Schmieder AH, Stacy AJ, Roessl E, Thran A, Wickline SA, Proska R, Lanza GM. An Early Investigation of Ytterbium Nanocolloids for Selective and Quantitative "Multicolor" Spectral CT Imaging. ACS Nano. 2012; 6:3364–3370. [PubMed: 22385324]
207. Liu Y, Ai K, Liu J, Yuan Q, He Y, Lu L. A high-performance ytterbium-based nanoparticulate contrast agent for in vivo X-ray computed tomography imaging. Angewandte Chemie - International Edition. 2012; 51:1437–1442. [PubMed: 22223303]
208. Liu Y, Liu J, Ai K, Yuan Q, Lu L. Recent advances in ytterbium-based contrast agents for in vivo X-ray computed tomography imaging: Promises and prospects. Contrast Media and Molecular Imaging. 2014; 9:26–36. [PubMed: 24470292]
209. Liu Z, Li Z, Liu J, Gu S, Yuan Q, Ren J, Qu X. Long-circulating Er 3+-doped Yb 2O 3 up-conversion nanoparticle as an in vivo X-Ray CT imaging contrast agent. Biomaterials. 2012; 33:6748–6757. [PubMed: 22770569]
210. McDonald RJ, McDonald JS, Newhouse JH, Davenport MS. Controversies in Contrast Material-induced Acute Kidney Injury: Closing in on the Truth? Radiology. 2015; 277:627–632. [PubMed: 26599922]
211. Davenport MS, Cohan RH, Ellis JH. Contrast media controversies in 2015: imaging patients with renal impairment or risk of contrast reaction. AJR. American journal of roentgenology. 2015; 204:1174–1181. [PubMed: 25730301]
212. Diehl K-H, Hull R, Morton D, Pfister R, Rabemampianina Y, Smith D, Vidal J-M, Vorstenbosch CVD. A good practice guide to the administration of substances and removal of blood, including routes and volumes. Journal of Applied Toxicology. 2001; 21:15–23. [PubMed: 11180276]
213. Leander P, Höglund P, Børseth A, Kloster Y, Berg A. A new liposomal liver-specific contrast agent for CT: first human phase-I clinical trial assessing efficacy and safety. Eur Radiol. 2001; 11:698–704. [PubMed: 11354769]

214. Morcos S. Acute serious and fatal reactions to contrast media: our current understanding. Br J Radiol. 2014

215. De Cecco, CN., Laghi, A., Schoepf, UJ., Meinel, FG. Dual Energy CT in Oncology. Springer; 2015.

216. Roessler AC, Hupfer M, Kolditz D, Jost G, Pietsch H, Kalender WA. High Atomic Number Contrast Media Offer Potential for Radiation Dose Reduction in Contrast-Enhanced Computed Tomography. Investigative radiology. 2016; 51:249–254. [PubMed: 26606552]

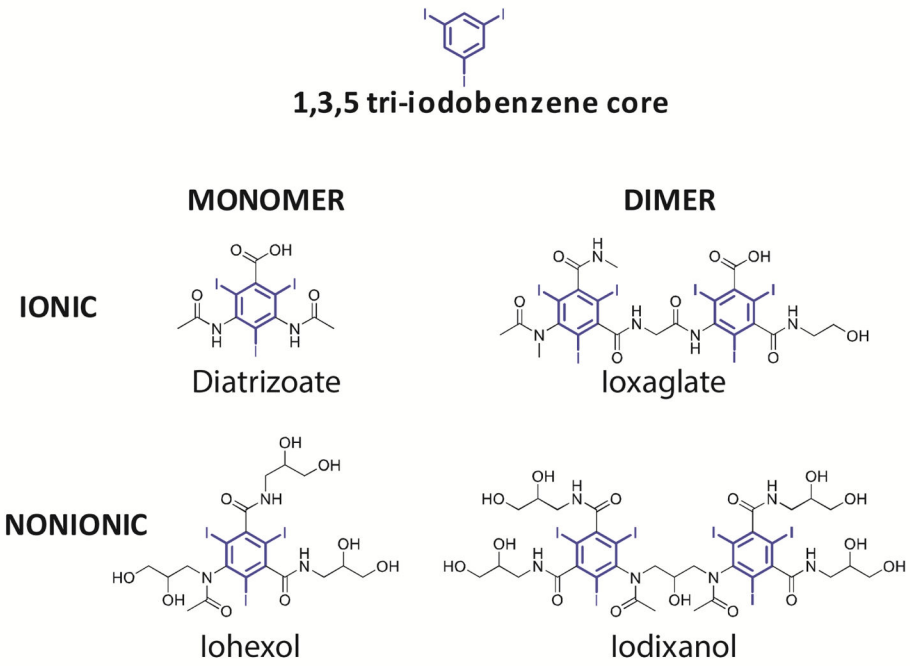

Fig. 1.

Iodinated contrast material examples. (Top row:) All current general purpose CT contrast materials are based on the 1,3,5 tri-iodinated benzene core. (Middle row:) Ionic contrast materials, such as diatrizoate, showed higher osmolality and toxicity than (Bottom row:) Nonionic contrast materials which had lower osmolality. Dimeric tri-iodobenzene contrast materials allowed for even lower osmolality such that formulations could be iso-osmolar to blood.

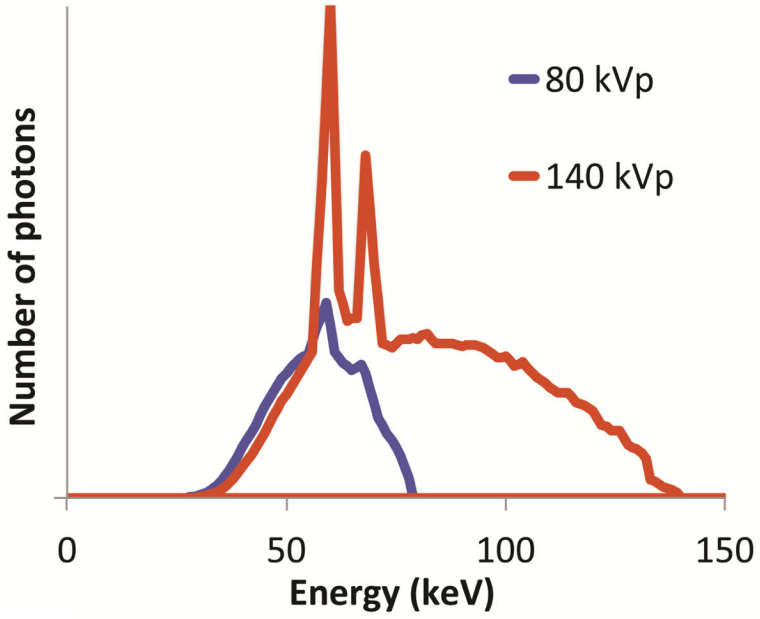

Fig. 2.

The X-ray spectra for CT X-ray tube voltages of 80 and 140 kVp of a clinical CT scanner. The maximum photon energy for the 80 kVp tube voltage setting is 80 keV, and that for 140kVp is 140 keV.

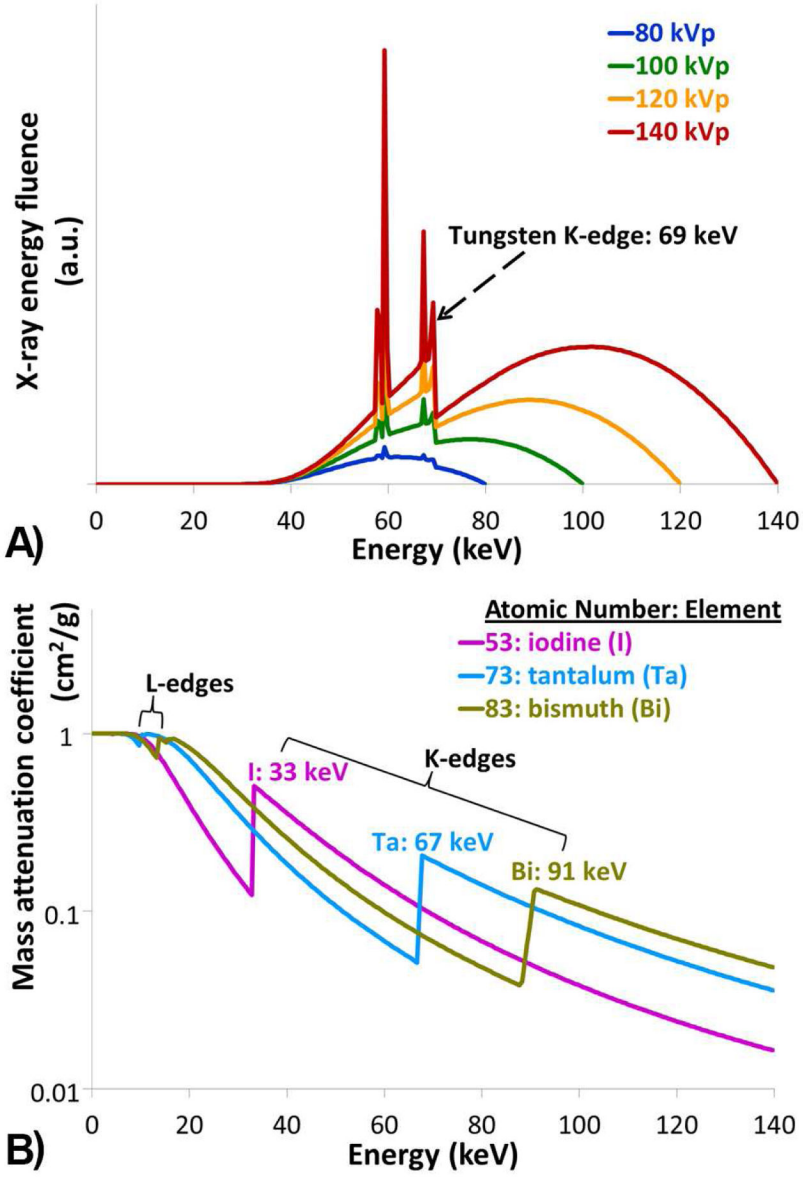

Fig. 3.

(A) The X-ray spectra for X-ray tube voltages (kVp) most commonly used at CT are depicted. These were simulated using typical CT system parameters, constant X-ray tube current (mA), and a medium-large patient size; the spectra represent the energy at the detector. Note that at the same mA, the higher-kVp spectra contain much more energy than the lower-kVp spectra. The substantial drop in fluence above approximately 69 keV is due to the self-filtration of the tungsten anode of the X-ray tube; the K-edge of tungsten causes a sharp increase in attenuation of X-ray photons above tungsten's 69-keV K-edge energy, and a corresponding decrease in X-ray energy leaving the anode. (B) The mass attenuation coefficients (MAC; μ/ρ; cm^2/g) are shown for three representative materials. Iodine's K-edge energy (33 keV) is at the lower limit of all of CT's energy spectra; tantalum's 67-keV K-edge energy is within all of the CT spectra; bismuth's 91-keV Kedge energy is too high to

produce good attenuation with the 80- and 100-kVp spectra, but it is within the 120- and 140-kVp spectra. However, bismuth's L-edge at 16 keV increases its low-energy attenuation above that of iodine and tantalum, until the K-edges of the latter elements boost their attenuation above that of bismuth.

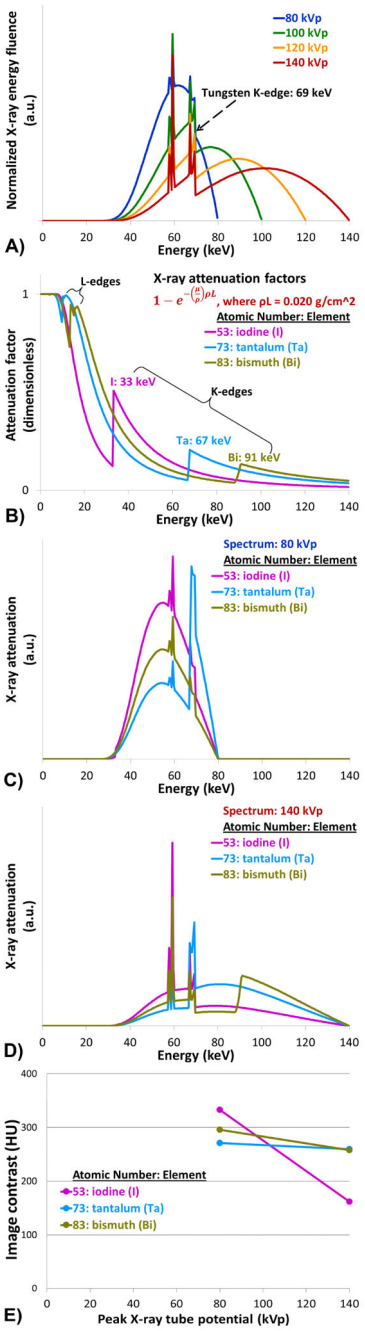

Fig. 4.

(A) The X-ray spectra of Fig. 3A, shown normalized to constant integrated energy. (B) The "attenuation factor" $1\text{-}e^{-(\mu/\rho)\rho L}$, for active element concentration (ρ) of 10 mg/mL and path length (L) of 2 cm. (C) The product of the 80-kVp spectrum from (A) and the attenuation factors from (B), representing the energy attenuated by those elements when the 80-kVp spectrum is used. The total attenuated energy is highest for iodine, but the large increase in tantalum's attenuation at its 67-keV K-edge results in a total attenuation that is similar that of bismuth. (D) The product of the 140-kVp spectrum from (A) and the attenuation factors

from (B), representing the energy attenuated by those elements when the 140-kVp spectrum is used. The total attenuated energy is highest for tantalum, but the large increase in the attenuation of bismuth due to its 91-keV Kedge results in a total attenuation that is higher than that of iodine. With the 140-kVp spectrum, iodine has a lower attenuation than tantalum or bismuth. (E) The empirically-measured CT image contrast that results from the examples presented above. The material concentration was 10 mg of active element per milliliter of aqueous solution, with the sample placed in the center of a 32-cm CT dose index phantom. Data from Fitzgerald et al, Radiology 2016.

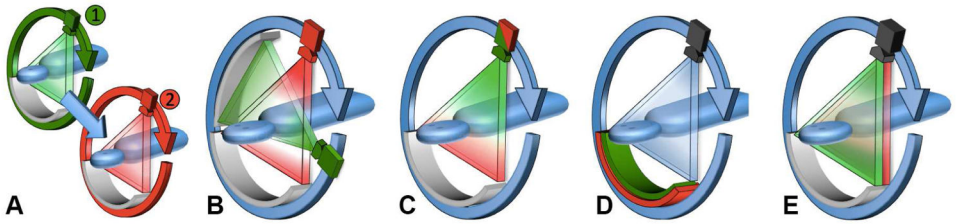

Fig. 5.

Schematic diagram of the operating principles for the different clinical dual-energy CT platforms currently available. A) Rotate-rotate CT, where sequential low- and high-energy acquisitions are obtained. B) Dual Source CT, where low- and high- energy data is acquired using two X-ray source and detector pairs. C) Rapid-kVp-switching CT, where the tube potential of a single X-ray source is rapidly switched between low- and high-energies. D) Multilayer detector CT, where the front layer of a sandwich detector preferentially absorbs low-energy X-ray photons, while the back layer absorbs the remaining high-energy X-ray photons. E) Split-beam CT, where a two-part filter mounted along the patient axis length modulates the X-ray spectra into a high- and low-energy spectrum for each half of the beam from a single non-switching source.

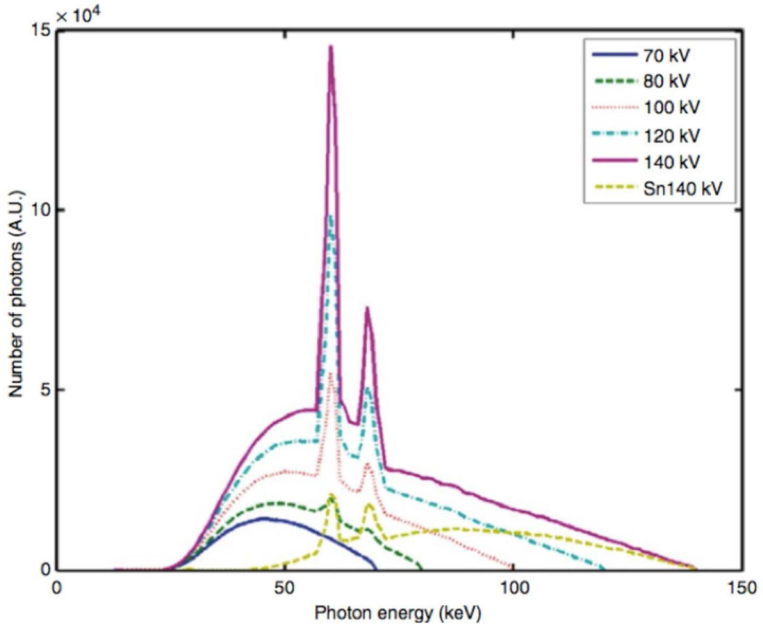

Fig. 6.

Typical X-ray spectra used in medical CT. Representative spectra at 70, 80, 100, 120, and 140 kVp, after standard pre-filtration, are shown. Their mean energies range between 47 and 69 keV. The Sn kV spectrum is obtained after pre-filtration with 0.4 mm Sn (tin) to preferentially remove lower energy X-ray quanta and shift the mean energy of the spectrum to higher values. Image from page 4 of [215].

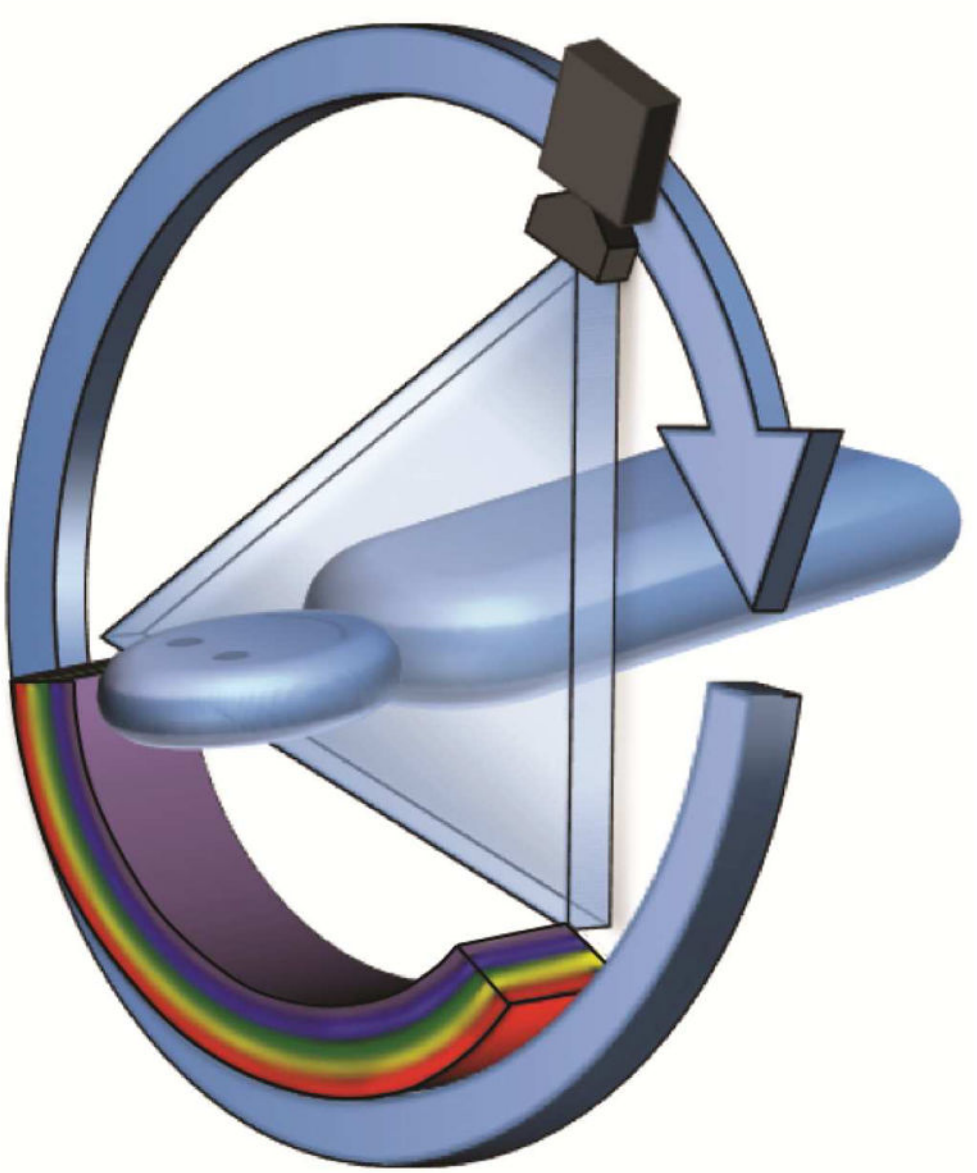

Figure 7a

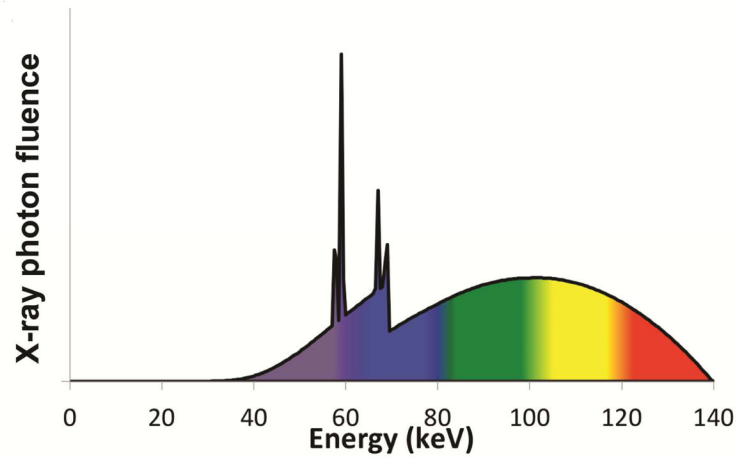

Figure 7b

Fig. 7.

A) Conceptual diagram of the operating principle of a CT system that incorporates a photon-counting, energy-discriminating (PCED) detector. In order to generate energy-specific projection data, PCED detectors ideally detect each individual incoming X-ray photon, characterize the photon's energy, and increment a counter associated with a specific energy range (or bin) encompassing the energy of the photon. In this figure, the corresponding colors in the B) spectrum and the A) detector represent ranges of energies associated with the detector's energy bins. To be clear, PCED detectors are not physically layered, but do record the number of detected photons within one of several energy bins. Therefore, the precision of energy discrimination is superior to that of multilayer-detector CT.

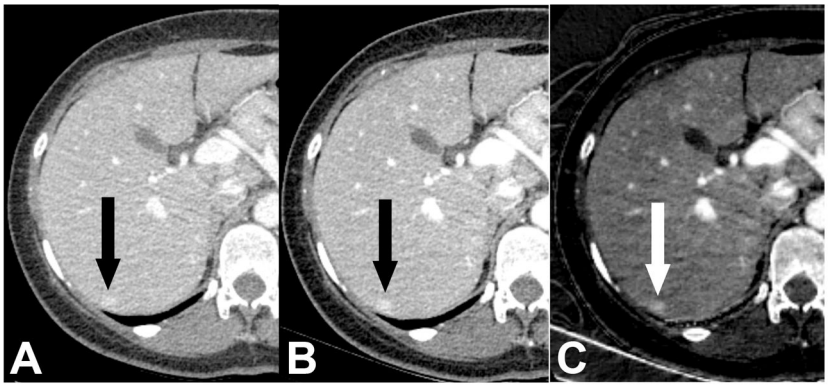

Fig. 8.

Intravenous contrast-enhanced DECT scan of the liver. A) A subtle hyperenhancing focus (arrow) is faintly seen on the standard transverse CT image reconstruction. B) The lesion is more conspicuous on the virtual monoenergetic low keV (52 keV) image and C) iodine density map. These types of DECT reconstructions improve lesion detection for both hyper- and hypovascular lesions.

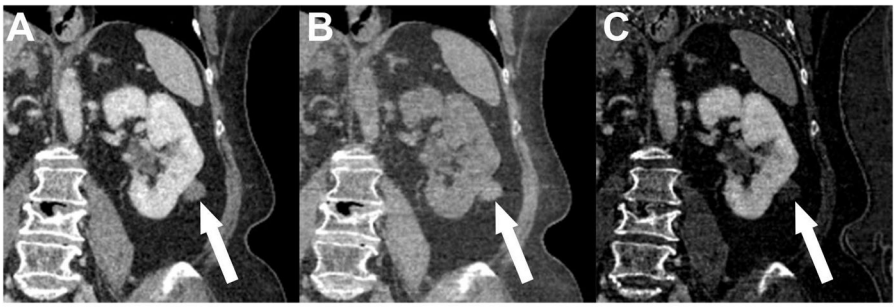

Fig. 9.

Kidney mass imaged at DECT. a) Portal venous phase coronal CT image shows a high density renal mass (arrow) that is ambiguous for enhancing tumor versus a hemorrhagic cyst. The DECT scan material decomposition images show B) high density in the lesion on the water / virtual unenhanced image without high density in the C) iodine density image. These findings confirm that the lesion does not enhance with intravenous contrast material and is not a renal cell carcinoma. Instead, the lesion is diagnosed as a benign hemorrhagic cyst and requires no further follow up. Were it not for the material decomposition images, additional imaging workup would have been required for this patient to assess for enhancement.

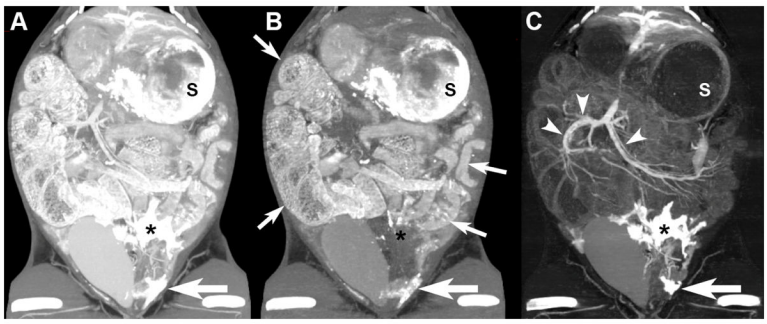

Fig. 10.

Double contrast-enhanced DECT scan with tungsten enteric and intravenous iodinated contrast material in rabbit with sharp abdominal trauma. A) Standard CT reconstruction shows a leak of contrast material (asterisk *) in the lower abdomen and another in the pelvis (large arrow), ambiguous for perforated bowel versus bleeding. B) Tungsten image from same scan shows contrast opacification of bowel lumen (small arrows) and in the pelvic leak, confirming a bowel perforation. No oral contrast is seen in the abdominal leak. C) Iodine density map shows the blood vessels (arrowheads) well, and confirms that the abdominal leak is due to bleeding rather than leaked bowel contents, and also shows bleeding into the pelvic leak. Such clarity for the diagnosis of injury is not possible with conventional SECT. S=stomach

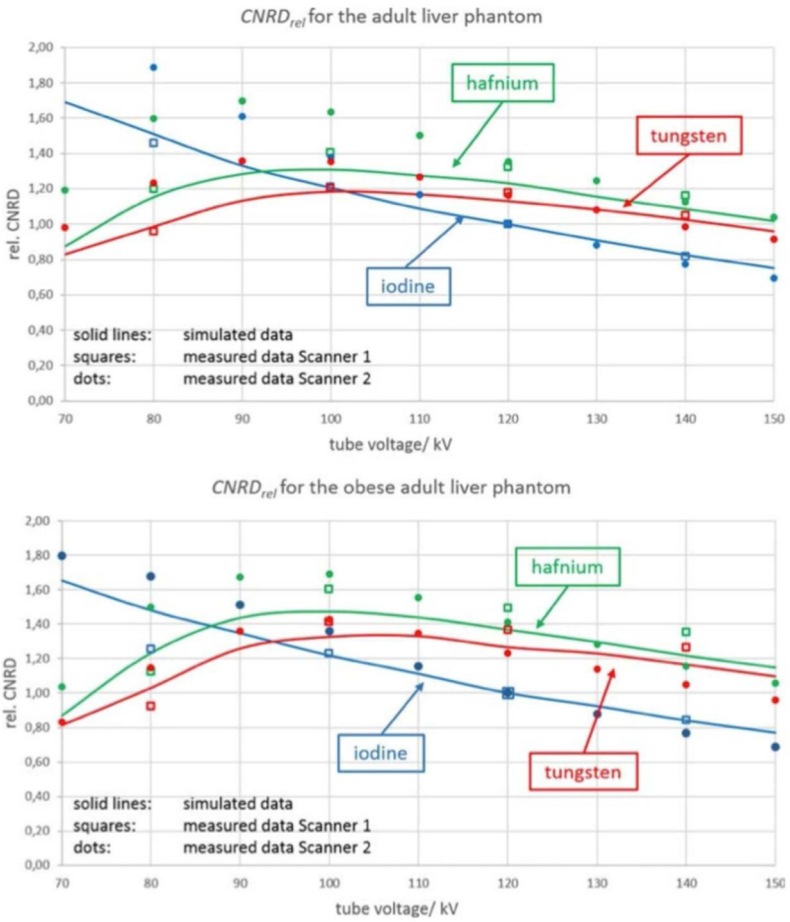

Fig. 11.

Simulated dose-weighted contrast-to-noise ratio (CNRDrel) and measured CNRDrel of iodine versus hafnium and tungsten in an adult liver phantom and an obese adult liver phantom at different kVp in a clinical CT scanner. Image from [216].

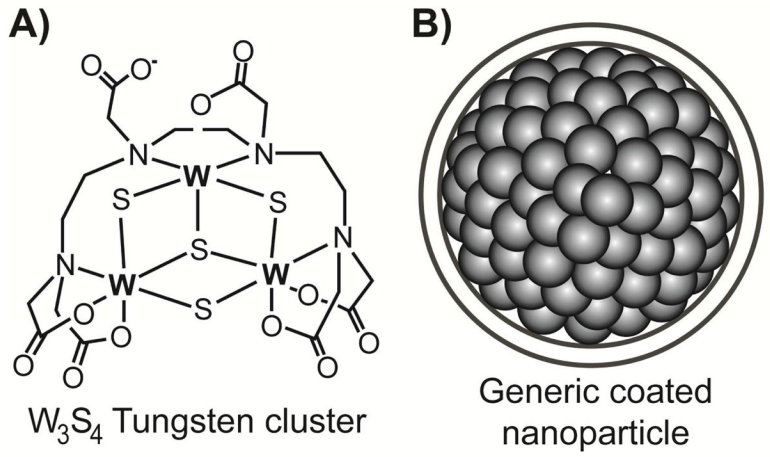

Fig. 12.

Potential biocompatible constructs for non-iodinated contrast materials. A) X-ray attenuating elements can be tightly bound in a small molecule cluster configuration, such as this W_3S_4 tungsten cluster. Much like tri-iodinated benzene rings, such clusters may be linked to targeting moieties to change their biodistribution. B) Densely packed nanoparticles of X-ray attenuating elements provide high X-ray attenuation since thousands of X-ray attenuating atoms may be present per particle. Biocompatible coatings are generally applied to these nanoparticle contrast materials to improve their safety profiles and to link the nanoparticles to targeting moieties.

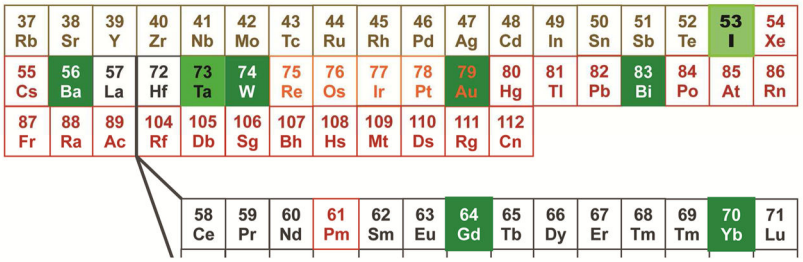

Fig. 13.

Potential of chemical elements for use as general purpose DECT contrast materials. Also, see corresponding Table 1.

Red: Low potential due to toxicity, radioactivity, or gaseous phase.

Brown: Low practical potential due to low X-ray attenuation, poorer than that of iodine and similar to that of biological tissues.

Orange: Little practical potential due to limited world production or high cost.

Gray: Moderate potential, but patient safety, availability, and cost for the anticipated composition and application needs to be explored.

Green background (all shades): Varying degrees of moderate to high potential; have been used clinically or are reported in the literature as candidates for consideration as CT contrast materials.

Light green (iodine): The only current clinical general purpose CT contrast material.

Medium green (tantalum): Currently under investigation as a general purpose CT contrast material.

Dark green: Have important limitations such as potential toxicity or low world production quantity that may prohibit widespread use as a general-purpose CT agent.

Table 1

Characteristics of candidate elements for CT contrast agents [46–49]. Please see legend of Fig. 13 for notations on highlighted and colored text.

Atomic number (Z)	Name	Symbol	K edge (keV)	Annual production (metric tons)	Raw cost of material per 30 g dose (USD)		Concerns*
53	**Iodine**	**I**	**33.2**	**>30,000**	**<1**		**I >100 kVp**
56	**Barium**	**Ba**	**37.4**	**6,000,000**	**<1**	**BaSO4**	**T for IV**
57	Lanthanum	La	38.9	12,000	<1	La_2O_3	
58	Cerium	Ce	40.4	23,000	<1	CeO_2	
59	Praseodymium	Pr	42.0	2,500	<1	Pr_6O_{11}	
60	Neodymium	Nd	43.5	7,000	<3	Nd_2O_3	
			45.2				
62	Samarium	Sm	46.8	700	<1	Sm_2O_3	A
63	Europium	Eu	48.5	100	<30	Eu_2O_3	C, A
64	**Gadolinium**	**Gd**	**50.2**	**400**	**<1**	**Gd2O3**	**T, A**
65	Terbium	Tb	52.0	10	<30	Tb_4O_7	C, A
66	Dysprosium	Dy	53.8	100	<20	Dy_2O_3	C, A
67	Holmium	Ho	55.6	10	<1	Ho_2O_3	A
68	Erbium	Er	57.5	500	<1	Er_2O_3	A
69	Thulium	Tm	59.4	50	<1	Tm_2O_3	A
70	**Ytterbium**	**Yb**	**61.3**	**50**	**<1**	**Yb_2O_3**	**T, A**
71	Lutetium	Lu	63.3	10	<50	Lu_2O_3	C, A
72	Hafnium	Hf	65.3	50	<20	HfO_2	C, A
73	**Tantalum**	**Ta**	**67.4**	**>1,200**	**<1**	**Ta_2O_5**	**I <90 kVp**
74	**Tungsten**	**W**	**69.5**				**T**
79	**Gold**	**Au**	**80.7**	**2,800**	>1,000		**C, I**

Atomic number (Z)	Name	Symbol	K edge (keV)	Annual production (metric tons)	Raw cost of material per 30 g dose (USD)	Concerns*
83	Bismuth	Bi	90.5	8,500	<1	I

*G – Gas; no stable solid compounds at room temperature
T – Toxicity
C – Cost
A – Availability
I – Imaging performance
R – Radioactivity (toxic)